FLORIDA STATE UNIVERSITY
COLLEGE OF ARTS AND SCIENCES

DESCRIBING THE ONSET AND DEMISE OF THE AUSTRALIAN MONSOON

By
JOHN EDWARD UEHLING

A Thesis submitted to the
Department of Earth, Ocean, and Atmospheric Science
in partial fulfillment of the
requirements for the degree of
Master of Science

2019

John Uehling defended this thesis on July 2, 2019.

The members of the supervisory committee were:

Vasubandhu Misra

Professor Directing Thesis

Robert Hart

Committee Member

Allison Wing

Committee Member

The Graduate School has verified and approved the above-named committee members, and certifies that the thesis has been approved in accordance with university requirements.

TABLE OF CONTENTS

LIST OF TABLES

LIST OF FIGURES

ABSTRACT

A comprehensive rainfall-based index of the Australian monsoon is created. This index is based on methodology previously used on the Indian subcontinent for determining the seasonality of the Indian monsoon. In order to create the Australian monsoon index, only rainfall data is used, which even over the sparsely populated areas of northern Australia is available dating back over 100 years (to 1901). The methodology for calculating the Australian monsoon index has been shown to be robust and not susceptible to false onsets. The Australian monsoon index objectively captures the onset date, the demise date, and the total seasonal rainfall for each monsoon season.

This new index was then compared to various atmospheric dynamic and thermodynamic variables to see if the index was reflective of the broader seasonal atmospheric changes associated with the monsoon. The Australian monsoon index introduced in this study is found to be consistent with the meridional advancement of the precipitable water south of the equator and over the Australian land mass as the monsoon season begins. Atmospheric dynamics related to the low-level wind data shows a pronounced wind shift across the region corresponding to the onset and the demise of the monsoon based on the rainfall index.

The examination of linear trends show that the length of the season has gotten longer and wetter, with earlier onsets and later demises since the beginning of the 20th century. One final aspect of the monsoon that is investigated is the interannual variability of the monsoon and how the El Niño-Southern Oscillation (ENSO) impacts the onset, demise, length of season, and total rainfall of the Australian monsoon. It is observed that warm or cold ENSO events are associated with shorter or longer Australian monsoon season, respectively. Similarly, these warm or cold

ENSO events are associated with drier or wetter seasonal rainfall anomalies of the Australian monsoon, respectively.

CHAPTER 1

INTRODUCTION

The Australian monsoon, also known as the Indo-Australian monsoon, or the Asian-Australian monsoon, is a phenomenon where between the months of December and March, enhanced rainfall occurs over the northern region of the Australian continent (Wang 2002, Wyrtki 1960, Flohn 1960). During the austral summer months, east to northeasterly winds bringing moist air originating over the warm waters of the West Pacific Ocean and blow across northern Australia due to the increase in land-sea temperature contrast between the very warm Australian landmass and the relatively cooler tropical waters (Li et al. 2018). Atmospheric moisture being driven by these winds leads to a wet monsoonal season throughout the summer (Li et al. 2018). The vast majority of the annual rainfall for the northern regions of Australia occur during the summer months that comprise the Australian monsoon. These rains are extremely important to Australians as these rains are vital to their agricultural productivity and other related economic activity. In a continent that is as arid as Australia, the monsoon rains are naturally an important part of Australia's agricultural production. Due to the reliance on the monsoon rains for agricultural productivity by the Australians, having a thorough understanding of the monsoon's seasonality is vital.

The Australian monsoon is the strongest monsoon in the Southern Hemisphere and plays a vital role in the weather patterns of the region of northern Australia (Gallego et al. 2017). The strongest effects of the monsoon are felt in the domain covered between 30° S - 40°S, and 60° E - 160°E (Li et al. 2018). The Australian monsoon has been of interest to meteorologists in Australia for many decades due to its importance in the region (Wang 2002, Wyrtki 1960).

Having a comprehensive understanding of the seasonality of the monsoon and how this seasonality might be evolving with time would provide vital information to residents of Australia to help plan for anomalous monsoon seasons (Meehl et al. 1998).

Reliable rainfall records vary depending on where you are and in the case of Australia reliable rainfall records go back to the late 1800s, but these records lack complete expansive coverage of the continent (Australian Bureau of Meteorology, 2018). Numerous studies have been conducted about the seasonality of the Australian monsoon, with different indices being developed using various methodologies to determine the onset and the demise of the Australian monsoon. One such index uses the 850 hPa zonal wind averaged over the area between 5° S – 15° S, 110° E – 130°E to derive the Australian monsoon index (AUSMI; Kajikawa 2009). AUSMI has been used to characterize the seasonal cycle of the monsoon, including factors such as intraseasonal variations, interannual variations, and even interdecadal variations in the monsoon (Kajikawa 2009). As mentioned however, the AUSMI only takes into account the wind patterns within a rather limited domain area and does not take into account how much rain has actually fallen on the Australian subcontinent. The AUSMI has proven to be a useful metric in previous studies, and significant correlations have been found between the monsoon onset date and the mean AUSMI anomalies during the peak of monsoon season between December and February (Kajikawa 2009). In a similar study conducted in 2004, the 850 hPa winds had been averaged over the region between 0° - 10° S, 120° E – 150° E to derive a similar index defining the Australian monsoon (Wang et al. 2004). This methodology however ignores the rainfall data from northern Australia, and as such ignores a critical component of the monsoon. The rainfall is what is most important societally, thus defining a monsoon index using rainfall data from northern Australia is arguably much more useful.

Determining the exact onset and the demise of the monsoon is incredibly important, as this information is vital for human and environmental interests such as farming and water resource management. Due to its importance, many studies have been previously conducted with the intent of delineating the exact monsoon season. One of the earliest studies analyzed variations in upper tropospheric flow that was associated with the onset of the Australian monsoon (Troup, 1961). Later studies began looking at rainfall data at the city of Darwin (located in northern Australia, with reliable rainfall records dating back to the 1800s), to analyze the onset and demise of the Australian monsoon (Nicholls et al., 1982; Holland. 1986). Other studies have looked at historical wind records recorded at the city of Darwin to derive the seasonality of the Australian monsoon (Drosdowsky, 1996; Holland, 1986). These previous works were all quite important as they all presented a methodology of defining the seasonality of the Australian monsoon, but they all suffer from an issue regarding the scope of their dataset. The region of Australia that is impacted by the monsoon is much larger than just the area around the city of Darwin. As previously mentioned the monsoonal region can be defined by a box bounded approximately between 0° – 15° S, 110° E – 150°E. The heaviest rainfall associated with the Australian monsoon occurs between 7.5° S – 17.5° S and 120° E – 150° E (Kajikawa, 2009). This provides a useful domain for analyzing the rainfall data over northern Australia.

Previous studies have been limited in their scope to simply analyzing wind data or just the rainfall at the city of Darwin. Due to these limitations, previous indices do not provide a wholistic viewpoint of the Australian monsoon that includes both atmospheric and oceanic context. A more comprehensive analysis of the rainfall data over the entirety of northern Australia would likely provide a more robust characterization of the monsoon season. In a related study Noska and Misra (2016) introduced an index for the Indian summer monsoon that

uses the All-India rainfall (Noska, 2016). This methodology uses just the rainfall data from across the Indian subcontinent to derive a simple index, the All-India rainfall onset and demise (AIROD), to determine the onset and demise of the Indian summer monsoon. This index is found to be extremely robust (Noska, 2016). This methodology would be easily translated to the northern Australian region to create and define a new monsoon index that uses simply the rainfall data across the monsoonal region that could be used to describe accurately the seasonality of the Australian monsoon.

Another limitation of previous indices not yet mentioned is that false onsets can occur. A false onset is when there is a temporary increase in rainfall that is followed by a period of dryness prior to the true beginning of the monsoon season (Joseph et al., 1994). Using rainfall data over a large domain such as all of northern Australia provides a greater likelihood of avoiding such false onsets. False onset events are triggered by small-scale convective events (e.g. isolated thunderstorms or squall lines) that are followed by extended dry spell. In taking an area average over a region like over northern Australia to define this index of the monsoon, it is unlikely to isolate such small scale events and may be regarded as a large-scale index of the Australian monsoon. The new index that is presented here uses the methodology described by Noska and Misra (2016) and uses the northern Australian rainfall (NAR) only to create the Northern Australia monsoon onset and demise index (NAMODI).

This index is proposed primarily to integrate the rainfall data across the entire northern Australian domain into a more robust and comprehensive monsoon index that can be used to determine the seasonality of the Australian monsoon. This new index is simple in the fact that it only uses rainfall data. The rainfall dataset for the northern Australian region is robust (quality

controlled) and dates back to the year 1900, and this index (as defined in this study) is less susceptible to the false onsets that could occur as a result of using previously defined methods.

This newly proposed methodology for defining an Australian monsoon index can be used to capture interannual variability, the seasonal evolution of the monsoonal cycles, and is even robust enough to avoid the issue of false onsets. This methodology can be easily implemented to accurately describe all past monsoon events (so long as accurate rainfall data is available.

CHAPTER 2

DATA

The data used in this study was sourced from the Australian Bureau of Meteorology's rain gauge network across the Australian continent. The Bureau of Meteorology has rain gauges across the continent, and that data was then compiled to help form the dataset. The dataset itself is on a 0.5° grid, with complete coverage of the Australian landmass (Grant, 2012). The dataset however does not include any ocean areas at all, and all the valid grid points are solely over land areas. The data ranges from January 1, 1900 through until December 31, 2015 (Grant, 2012). This time period represents 115 years of available station data, which helps improve the robustness of the study. 115 years of data provides an ample time period to gauge the climatology and the seasonality of the Australian monsoon with a high degree of certainty about the conclusions. The dataset used in this study uses the term 'rainfall' when describing any form of precipitation. The data itself included frozen precipitation in the data, which has been converted to liquid water equivalent (Grant, 2012). This ensures that there is no missing precipitation in the dataset due to the precipitation being frozen. For the purposes of this study 'rainfall' and 'precipitation' both will refer to total precipitation accumulation (both frozen and not frozen).

Over time the Australian rain gauge network has changed, and it is more complete now than it was at the beginning of the dataset period. Figure 2 shows how the rain gauge distribution at the current time, which is much more dense than the distribution in 1900, at the beginning of the dataset.

The rainfall data as mentioned before comes from the Australian Bureau of Meteorology, which is recorded in the Australian Data Archive for Meteorology (ADAM). The 24 hour daily period used runs between 9 AM of the previous day through to 9 AM of the current day, using the local time of the site of the gauge.

One other important note about the dataset is that the Bureau of Meteorology updates the dataset continuously, performing quality control for the data, which ensures high quality data (Grant 2012). The Bureau of Meteorology has extensively quality controlled the data, to ensure its reliability (Grant, 2012). This ensures that the gridded dataset is as accurate as possible, and that the data in this study is therefore an optimal dataset to use.

As mentioned previously, the dataset itself is on a spatial grid with a 0.5° resolution. The rain gauge network does not align perfectly with this grid, and thus an algorithm was needed to transpose the rain gauge data onto the grid. The grids were generated using a sophisticated technique that comes from a methodology using an optimized Barnes successive correction technique (Jones et al., 2009). This methodology applies a weighting average to each of the stations over Australia which can then be extrapolated to fit the grid (Grant, 2012). The dataset is also decomposed into a long-term average component and also an anomaly component (Grant, 2012).

Grant (2012) mention some limitations of the dataset that are important. The data grid itself could not be any more precise due to the sparseness of gauges (in particular in the outback and other more rural areas), which does limit the accuracy of the data somewhat. In the case of this study, shouldn't be of major concern due to the relatively dense observation network over the area of northern Australia in question. Grant (2012) also points out that in regions with a

high observational density, or where there are strong gradients, the data-smoothing technique applied to the data could potentially result in certain grid-point values that differ from the rainfall amounts at the contributing stations (Grant 2012).

Lastly calculations have been performed to determine the accuracy of the spatial analyses used to create the gridded dataset used in this study. The results concluded that the daily rainfall values have a root mean square error of 3.1 mm and a mean absolute error of 0.9 mm (Grant, 2012). This shows that the data itself is quite accurate (values are generally accurate to within 0.9 mm) and thus the results of the study should be taken to be more definitive due to the certainty surrounding the accuracy of the data used.

Additionally, other atmospheric variables were also analyzed from the climate forecast system reanalysis (CFSR; Saha et al. 2010), which has global atmospheric data dating back to 1979. This reanalysis data has superior resolution to previous NCEP reanalyses and accounts for changing CO_2 and other trace gases, aerosols, and solar variations (Saha et al. 2010). This atmospheric reanalysis data was used to compute various aspects of how different dynamic and thermodynamic variables changed during the onset and demise periods of the Australian monsoon. The data used came from the region from the equator to 30°S and from 100°E to 160°E, and each year from 1979 to 2010 was used.

CHAPTER 3

METHODOLOGY

Defining the all-Australia rainfall monsoon onset and demise index

For this study the onset and demise of the Australian monsoon was computed using only daily rainfall data from northern Australia. The methodology is the same as was used in past studies looking at the Indian monsoon. Per Leibmann et al. (2007), Misra and DiNapoli (2014), and Noska and Misra (2016), the daily anomaly was calculated by using the equation,

1.) $Cumulative\ Daily\ Anomaly = \sum_{i=1}^{n}(DRF(n) - \overline{CDRF})$

where DRF(n) is the daily rainfall of the nth day for a given year averaged over the northern Australian monsoon region (Figure 1). $\overline{CDRF}$ is the annual mean climatology averaged over northern Australia and is calculated over the entire time period between 1900 and 2015.

Once this calculation was performed, the onset and demise for any particular year could be found by simply looking at the first day after the day in which the absolute minimum of the cumulative daily anomaly was reached (which is the onset date). This is due to the fact that prior to the onset of the monsoon, the daily rainfall is typically less than the average daily rainfall for the entire 1900-2015 time period. This results in the curve decreasing until the date of onset, at which point the daily rainfall is typically more than the average daily rainfall for the entire 1900-2015 time period. This results in the minima in the cumulative anomaly curve representing the onset. Similarly, the day after the absolute maximum of the cumulative daily anomaly is defined as the demise date. The maxima of the curve is reached because post-demise, the daily rainfall values typically do not exceed the average daily rainfall for the entire 1900-2015 time period.

For the purpose of illustration, Figure 3 shows the time series of the daily rainfall overlaid with the cumulative anomaly curve for the year 1990. These inflection points in the cumulative anomaly curve translate to the first day of the year when the annual mean climatological rainfall is exceeded for onset and the last day of the year when the rainfall falls below the annual mean climatological rainfall for demise of the Australian monsoon. The length of each monsoon season calculated is shown in table 1.

A Mann Kendall analysis was then performed on each of the trends to determine whether the trend was statistically significant. In each figure for the linear trends of the monsoon over time, this analysis was performed, and the results shown in the figure captions. A Mann Kendall analysis is performed because it states that the null hypothesis is that there is no trend, thus if the null is able to be rejected at a certain confidence level, it means that there is in fact a linear trend in the data.

CHAPTER 4

RESULTS

Linear trends in the evolution of the monsoon

The rainfall index of the Australian monsoon was computed for all 115 years. The monsoon seasonal length lasts an average of approximately 115 days, but there is significant variance amongst the varying seasons. The standard deviation about the mean is 29.5 days, which is almost a full month of variance. The full range of seasonal lengths varies from the shortest season (the 1901-1902 season) being only 31 days long, to the longest season (2010-2011) being 191 days long. This means that over the last 115 years the range of monsoon season lengths has had a range of 160 days. In order to analyze how the seasonality of the Australian monsoon has evolved since 1900, the length (Figure 4) and corresponding onset date (Figure 5) and demise data (Figure 6) was plotted as a time series. The values themselves for each season can be found in table 2. The time series clearly indicates a strong linear trend in all three parameters that passes the Mann Kendall test at 99% significance level. These figures suggest that length of the season is increasing at the rate of 0.338 days/year (Figure 4), the onset date of the Australian monsoon is occurring earlier at the rate of 0.180 Julian day/year (Figure 5), and the demise date is occurring later at the rate of 0.153 Julian day/year (Figure 6). On account of these changes to the evolution of the Australian monsoon there is also a consequent increasing linear trend in the accumulated seasonal rainfall (Figure 7). As the length of the Australian monsoon has increased over time, the seasonal accumulation of rainfall has also increased. However, it is not obvious if this linear trend in seasonal accumulation of rainfall in Figure 7 is a result of the increasing length of the season, an increasing daily rain rate or a combination of

both. In order to resolve this issue we examined the seasonal rain in units of daily rain rate (=accumulated seasonal rain/ length of the season) in Figure 8 and found a similar increasing trend of 0.015 mm/day/year. This result in Figure 8 clearly suggests that the Australian monsoon season has increasing accumulation of seasonal rain from a combination of both increasing length of the season and the increasing daily rain rate. Table 3 shows the computed values for each monsoon season in terms of accumulated rainfall and also the rainfall rate. It is worth noting that due to the heterogeneity of the station data used, the resulting trends could potentially be impacted and inflated. This said however, looking at just 1960 onwards and there is still a strong positive trend in both total seasonal rainfall accumulation (3.2 mm/season/year) and rainfall rate (0.44 mm/day/year). Both trends also pass a Mann Kendall test at 99% significance. This suggests that station heterogeneity alone does not account for the trends seen in the rainfall data.

The average onset date for a typical northern Australian monsoon over the 115 years of study was the 341st day of the year (early December). As with the mean of the season length, the average onset date of the monsoon does not tell a complete picture. There is a significant variance about the mean in association with the onset dates of the monsoon. The standard deviation of the onset dates about the mean is 18 days, which is a significant variance (more than half a month). The earliest onset date over the entire time period occurred during the 2010-2011 monsoon season, and the onset day that year was October 8th (Julian day 281). The latest start to a monsoon season between 1900-2015 occurred during the 1906 season. The onset date that year occurred on January 26th.

The demise dates of the monsoon show a very similar variance to the onset dates, with the standard deviation being about 19 days. The average demise date from 1900 to 2015 was the 91st

day of the year (late March/early April timeframe). As was previously mentioned, though the average demise date over the 115 years of study was the 91st day of the year, there was a wide variance, with notable outliers. The most notable outlier was the 1967-1968 monsoon season, which between 1900 and 2015 was the year with the latest demise date, occurring on May 27th (or the 148th day of the year). This year was unusual as most northern Australian monsoons have their demise occurring before mid-April. There are a few other notable late demise years, including the 1982-1983 season and the 1955-1956 season. There were notable early demise years as well, though most of the earliest demise years occurred towards the beginning of the 20th century, including the earliest demise during the 1900-2015 time period. The 1904-1905 monsoon season was the earliest to end, with the demise occurring on only the 42nd day of the year, February 11th.

Seasonal evolution of the monsoon

Area-averaged rainfall was calculated for the period from 30 days prior to onset to 30 days after the onset of each monsoon. Figure 9 shows the average spatial distribution of rainfall over northern Australia (in mm) for 30 days, 25 days, 20 days, 15 days, 10 days, 5 days, 1 day, and for the day of the onset of the northern Australian monsoon as well as the average spatial distribution of rainfall for 1 day, 5 days, 10 days, 15 days, 20 days, 25 days, and 30 days after the onset of the monsoon over the period from 1900 to 2015. These figures show the gradual southward migration of the precipitation band as the onset of the Australian monsoon approaches. After the onset of the Australian monsoon, the band of heavy precipitation remains over northern Australia (Figure 9). Prior to the onset of the monsoon typical rainfall values across the region were less than 3 mm/day on average. Beginning with the onset date most of the region had values exceeding 3 mm/day with isolated regions experiencing averages of over 10

mm/day during the typical monsoon onset period. The same composite was done for the demise period of the Australian monsoon as well with Figure 10 showing the average spatial distribution of rainfall over northern Australia (in mm) for 30 days, 25 days, 20 days, 15 days, 10 days, 5 days, 1 day, and for the day of the demise of the northern Australian monsoon as well as the average spatial distribution of rainfall for 1 day, 5 days, 10 days, 15 days, 20 days, 25 days, and 30 days after the demise of the monsoon over the period from 1900 to 2015. The panels in Figure 10 display a northward migration of the heavy precipitation as the demise date is approached. After the demise date of the Australian monsoon, the rains over northern Australia is substantially reduced. In contrasting Figures 9 and 10, we find that the changes pre and post demise are more abrupt than pre and post demise. For example, 5 days before the demise the rain rate over northern Australia is over 10mm/day and by day of demise the rain rate drops to below 2 mm/day on average (Figure 10). On the other hand, the changes around the onset date are more gradual (Figure 9).

The composite 850 mb wind is displayed over an area ranging from the equator to 30°S in latitude and from 100°E to 160°E in longitude (Figures 15 and 16). Figure 11 shows the streamlines of the 850 mb winds colored to show the velocities (in m/s) over the Australian region during the period from 30 days prior to the onset of the monsoon to 30 days after the onset of the monsoon. The individual days displayed are the same as what was displayed and calculated for the spatial rainfall distribution figures (Figures 9 and 10). The same was done for the 850 mb winds during the demise period of the monsoon and those results are shown in Figure 12. The anticyclonic flow dominates the pre-monsoon flow over Australia, which is gradually taken over by the cyclonic flow at the time of the onset and is completely dominated by the monsoon trough post onset (Figure 15). In the composites around the time of demise, the zonal

easterly flow further accelerates over northern Australia post demise relative to the pre demise period (Figure 16).

In order to get a more complete picture of the atmosphere during the onset and demise of the monsoon, the composite flow of the 200 mb winds are also displayed in the same manner as the 850 mb winds. Figure 17 shows the streamlines of the 200 mb winds colored to show the velocities (in m/s) over the Australian region during the period from 30 days prior to the onset of the monsoon to 30 days after the onset of the monsoon. The same thing was done for the demise period of the monsoon and shown in Figure 18. Figure 17 shows a strong, anticyclonic flow is established over northern Australia by time of onset and this flow pattern remains persistent thereafter. Similarly, the closed anticyclonic flow over northern Australia in the pre-demise period slowly transitions to a ridge in the post demise period (Figure 18).

In addition, using the wind data the 850 mb vorticity was also plotted for both the onset and the demise period of the monsoon as well. The vorticity was calculated by simply taking the vertical component of the curl of the meridional and zonal winds at the 850 mb level. The equation for vorticity is given by equation 2.

2.) $\zeta = \nabla \times \vec{u}$

Where $\vec{u}$ is the total wind.

Figure 19 shows the resultant 850 mb vorticity over the Australian region for the period from 30 days prior to onset of the monsoon to 30 days after the onset of the monsoon. The same calculations were also performed for the demise period and displayed in Figure 20. The line of positive, anticyclonic vorticity dominates in the pre-onset period, which gradually transitions to negative, cyclonic vorticity flow in the post-onset period (Fig. 19). Similarly, the line of

negative, cyclonic vorticity begins to recede from the pre-demise to post-demise period from northern Australia (Figure 20).

Lastly, the thermodynamic (temperature and moisture based) variables were investigated in a similar manner to the dynamic variables. First the average precipitable water was calculated for the period from 30 days prior to 30 days after both the onset and demise, as done with the previous variables and plotted in Figures 11 and 12. Prior to the onset, the atmospheric column over northern Australia is comparatively drier than the post-onset period (Figure 11). This contrast around the onset date of the monsoon is quite dramatic and consistent with the southward migration of the trough as the monsoon evolves. Similarly, the desiccation of the atmospheric column from pre-demise to post demise period over northern Australia is apparent in Fig. 12.

The evolution of the surface temperature in Figure 13 indicate the rising contrast between the ocean and land temperatures prior to onset that gets diminished post onset when the land temperature begins to cool while the ocean temperatures comparatively remain persistent. But in the composites around the demise of the monsoon in Figure 14, the land-ocean thermal contrast is further reduced post demise relative to pre-demise period.

Interannual variability

The interannual variability of the monsoon is important to analyze, as changes in large-scale features can have a very significant impact on how the Australian monsoon season changes from year to year. One of the most important large-scale phenomena globally is ENSO, and thus the relationship between ENSO and the Australian monsoon was comprehensively studied (Zhou

2009, Holland 1986). These studies suggest that there is a strong correlation between ENSO and the Australian monsoon, thus the relationship was further analyzed here.

First a scatterplot of the December through February mean Niño 3.4 sea surface temperature anomalies versus the onset day of the monsoon (in Julian Days) was created, which is shown in Figure 21. The R-squared value and the least squares fit line is shown in the figure. The values for the DJF sea surface temperature anomalies can be found in table 4. Table 5 shows the values with the trend removed. The scatter indicates that warm or cold DJF Niño3.4 SST anomalies is associated with later or earlier onset of the Australian monsoon, respectively. Similarly, Figure 22 shows the scatterplot of the December through February Niño 3.4 mean sea surface temperature anomalies against the demise day of the monsoon (in Julian Days). The R-squared value and regression line is shown in the figure. In contrast to Figure 21, the relationship in Figure 22 is weaker and suggests that warm or cold DJF Niño3.4 SST anomalies is associated with earlier or later demise of the Australian monsoon, respectively. Likewise, the scatter between DJF Niño3.4 SST anomalies and length of the monsoon season (Figure 23) suggests that warm or cold DJF Niño3.4 SST anomalies is associated with shorter or longer length of the season, respectively.

Additionally, the relationship of ENSO with the mean seasonal rainfall anomalies of the northern Australian monsoon is shown in Figure 24. This figure indicates a significant impact of ENSO on the Australian monsoon rainfall with warm or cold ENSO anomalies related with drier or wetter seasonal rainfall anomalies. In fact, this relationship shown in Figure 24 is made weaker if the seasonal rainfall anomalies of the Australian monsoon is based on fixed calendar months of December to Februrary (Figure 25). Therefore, accounting for the variations of the length of the Australian season is important to properly diagnose its teleconnection with ENSO

variability. Table 6 shows the December to February area averaged rainfall accumulation for each year from 1900-2011 (in mm) as well as the detrended DJF rainfall accumulation. Also included is the total monsoon season accumulated rainfall for each monsoon season from 1900-2011 (in mm) as well as the detrended data.

CHAPTER 5

CONCLUSION

The Australian monsoon rainfall index (AUSMRI) proposed in this paper is a robust and comprehensive index that objectively determines the onset and the demise of the monsoon while using only rainfall data. Since rainfall data is so widely available and has very reliable records over the region dating back to 1900, using just rainfall data to develop the index has numerous advantages. Due to its simplicity and the fact that it relies only on rainfall data, the AUSMRI can be easily used and interpreted moving forward. Additionally, this index by design reduces the likelihood of false onsets (usually triggered by isolated thunderstorm events or organized squall lines, which is followed by a pronlonged dry spell).

The true robustness of the AUSMRI can be seen when comparing the onset and demise dates derived from the index to various thermodynamic and dynamic atmospheric variables. The 850 mb winds show a very steady progression towards the onset of the monsoon season, with a very pronounced cyclonic flow around the northern Australian region for the entire period around the onset of the monsoon. This cyclonic flow pattern persists all the way through until the demise date where the cyclonic flow no longer persists at the 850 mb level. This shows that there is a wind shift associated with the AUSMRI's demise date for each monsoon season. When looking at the vorticity in the region during the onset period, a very clear and pronounced area of cyclonic vorticity can be clearly seen over the region, in correspondence with the onset of the monsoon. During the demise period the cyclonic vorticity, which initially covers much of the northern Australian region is replaced by anticyclonic vorticity after the demise date has

passed. The fact that these dynamic variables line up consistently with the onset and demise calculated from the AUSMRI show the validity of the index.

Thermodynamic variables were also looked at as well and compared to the AUSMRI onset and demise dates. Precipitable water data over the northern Australian region show that during the days leading up to the onset of the monsoon, the high values of precipitable water remain to the north of the Australian mainland. But once the onset date hits the monsoon region a marked increase in the precipitable water is observed over northern Australia. During the demise period, as calculated by the AUSMRI, the precipitable water values over northern Australia are relatively high until the demise date, after which the highest values retreat to the north towards the equator. The precipitable water shows that the AUSMRI seasons are consistently reflected by the thermodynamics of the region as well and further validates the index.

Another aspect that was analyzed was how the seasonality of the Australian monsoon has changed over time. The rainfall data for northern Australia shows that the length of the monsoon season has increased since 1900 from a length of around 95 days to a length of about 130 days now. This increase is season length corresponds to an average earlier onset date as well as a later demise date. The onset date at the beginning of the 20th century typically occurred around the 350th day of the year, whereas nowadays it typically begins around the 330th day of the year according to trends. A similar story can be seen with the demise date moving further back. At the beginning of the 20th century the demise occurred on average around the 82nd day of the year, whereas now it occurs on average around the 99th day of the year.

In addition to the monsoon season increasing in length, the average monsoon is producing more total rainfall and it is occurring at an increased rainfall rate. The rainfall data

suggests that since 1900 the average total rainfall over the course of a monsoon season has increased by approximately 300 mm per year, which is a substantial increase. Corresponding to this substantial increase in total rainfall is a similar increase in the rainfall rate, which has increased by about 1.6 mm/day since 1900. Both are very robust trends and the underlying cause of these trends will need to be more thoroughly investigated in future studies.

Finally, the impact on ENSO on the Australian monsoon was investigated, and it was shown that positive or negative sea-surface temperature anomalies during the December to February time period in the Niño 3.4 region of the Pacific (El Niño) tend to lead to later onset or earlier onset dates of the Australian monsoon, respectively. Additionally, positive DJF sea surface temperature anomalies in the Niño 3.4 region of the Pacific tend to correspond to overall shorter monsoon seasons over northern Australia. Positive values of DJF sea surface temperature anomalies in Niño 3.4 region of the Pacific also tend to produce less rainfall over the course of a monsoon season.

Additional studies of the Australian monsoon need to be conducted to better understand the trends in the length of the season with time as well as the cause of the increasing rainfall associated with each season. A more complete picture of the relationship between ENSO and the Australian monsoon is also needed to better understand the relationships between ENSO and the length of the monsoon season and the rainfall accumulations during each season. Also more investigations of how climate change will potentially impact the Australian monsoon would further add to our understanding of this phenomenon.

APPENDIX A

TABLES

Table 1: Year of monsoon and the length of that monsoon season in days.

Season	Length of Season (days)
1900-1901	80
1901-1902	31
1902-1903	85
1903-1904	136
1904-1905	58
1905-1906	46
1906-1907	121
1907-1908	108
1908-1909	79
1909-1910	146
1910-1911	166
1911-1912	102
1912-1913	96
1913-1914	111
1914-1915	93
1915-1916	108
1916-1917	130
1917-1918	104
1918-1919	79
1919-1920	88
1920-1921	136
1921-1922	95
1922-1923	122
1923-1924	97
1924-1925	139
1925-1926	88
1926-1927	129
1927-1928	110
1928-1929	109
1929-1930	76
1930-1931	137
1931-1932	94
1932-1933	135

Table 1 - continued

Season	Length of Season (days)
1933-1934	130
1934-1935	87
1935-1936	105
1936-1937	103
1937-1938	73
1938-1939	136
1939-1940	105
1940-1941	99
1941-1942	55
1942-1943	102
1943-1944	103
1944-1945	124
1945-1946	82
1946-1947	105
1947-1948	117
1948-1949	149
1949-1950	129
1950-1951	123
1951-1952	49
1952-1953	115
1953-1954	129
1954-1955	104
1955-1956	123
1956-1957	125
1957-1958	128
1958-1959	139
1959-1960	99
1960-1961	78
1961-1962	81
1962-1963	124
1963-1964	100
1964-1965	143
1965-1966	98
1966-1967	82
1967-1968	158
1968-1969	99

Table 1 - continued

Season	Length of Season (days)
1969-1970	103
1970-1971	151
1971-1972	142
1972-1973	111
1973-1974	156
1974-1975	131
1975-1976	123
1976-1977	136
1977-1978	139
1978-1979	134
1979-1980	101
1980-1981	100
1981-1982	146
1982-1983	160
1983-1984	138
1984-1985	135
1985-1986	114
1986-1987	64
1987-1988	113
1988-1989	164
1989-1990	154
1990-1991	92
1991-1992	101
1992-1993	90
1993-1994	105
1994-1995	133
1995-1996	139
1996-1997	98
1997-1998	116
1998-1999	179
1999-2000	181
2000-2001	174
2001-2002	102
2002-2003	73
2003-2004	109
2004-2005	107

Table 1 - continued

Season	Length of Season (days)
2005-2006	167
2006-2007	115
2007-2008	118
2008-2009	112
2009-2010	131
2010-2011	191
2011-2012	141
2012-2013	124
2013-2014	162
2014-2015	124

Table 2: Onset day and demise day of each Australian monsoon season from 1900-2015 as well as their corresponding Julian day. Note that onset days occur late in the year as the season spans the Austral summer.

Onset Day	Julian Day	Demise Day	Julian Day
December 31, 1900	366	March 21, 1901	080
January 2, 1902	002	February 12, 1902	043
January 5, 1903	005	March 31, 1903	090
December 7, 1903	341	April 21, 1904	112
December 15, 1904	350	February 11, 1905	042
January 26, 1906	026	March 13, 1906	072
November 13, 1906	317	March 14, 1907	073
December 12, 1907	346	March 29, 1908	089
January 4, 1909	004	March 24, 1909	083
November 20, 1909	324	April 15, 1910	105
November 6, 1910	310	April 21, 1911	111
December 9, 1911	343	March 20, 1912	080
December 26, 1912	361	April 1, 1913	091
December 11, 1913	345	April 1, 1914	091
December 7, 1914	341	March 10, 1915	069
December 4, 1915	338	March 21, 1916	081
December 1, 1916	336	April 10, 1917	100
November 14, 1917	318	February 26, 1918	057
December 24, 1918	358	March 13, 1919	072
December 17, 1919	351	March 14, 1920	074
November 22, 1920	327	April 7, 1921	097
December 16, 1921	350	March 21, 1922	080
December 6, 1922	340	April 7, 1923	097
December 9, 1923	343	March 15, 1924	075
November 29, 1924	334	April 17, 1925	107
December 30, 1925	364	March 28, 1926	087
November 23, 1926	327	April 1, 1927	091
December 11, 1927	345	April 3, 1928	094
December 18, 1928	353	April 6, 1929	096
December 24, 1929	358	March 10, 1930	069
November 25, 1930	329	April 11, 1931	101
December 23, 1931	357	March 26, 1932	086
December 11, 1932	346	April 25, 1933	115
November 26, 1933	330	April 5, 1934	095

Table 2 - continued

Onset Day	Julian Day	Demise Day	Julian Day
January 4, 1935	004	April 1, 1935	091
January 1, 1936	001	April 15, 1936	106
December 3, 1936	338	March 16, 1937	075
December 14, 1937	348	February 25, 1938	056
November 17, 1938	321	April 2, 1939	092
December 19, 1939	353	April 2, 1940	093
December 27, 1940	362	April 5, 1941	095
December 29, 1941	363	February 22, 1942	053
December 3, 1942	337	March 15, 1943	074
December 11, 1943	345	March 23, 1944	083
December 1, 1944	336	April 4, 1945	094
December 12, 1945	346	March 4, 1946	063
December 15, 1946	349	March 30, 1947	089
December 20, 1947	354	April 15, 1948	106
November 17, 1948	322	April 15, 1949	105
December 9, 1949	343	April 17, 1950	107
November 13, 1950	317	March 16, 1951	075
January 10, 1952	010	February 28, 1952	059
December 25, 1952	360	April 19, 1953	109
December 18, 1953	352	April 26, 1954	116
December 4, 1954	338	March 18, 1955	077
January 7, 1956	007	May 9, 1956	130
December 8, 1956	343	April 12, 1957	102
December 10, 1957	344	April 17, 1958	107
November 22, 1958	326	April 10, 1959	100
December 18, 1959	352	March 26, 1960	086
December 17, 1960	352	March 5, 1961	064
December 14, 1961	348	March 5, 1962	064
December 17, 1962	351	April 20, 1963	110
December 19, 1963	353	March 28, 1964	088
November 8, 1964	313	March 31, 1965	090
December 3, 1965	337	March 11, 1966	070
January 1, 1967	001	March 24, 1967	083
December 21, 1967	355	May 27, 1968	148
December 20, 1968	355	March 29, 1969	088
December 11, 1969	345	March 24, 1970	083

Table 2 - continued

Onset Day	Julian Day	Demise Day	Julian Day
November 24, 1970	328	April 24, 1971	114
November 26, 1971	330	April 16, 1972	107
December 31, 1972	366	April 21, 1973	111
November 6, 1973	310	April 11, 1974	101
December 3, 1974	337	April 13, 1975	103
November 24, 1975	328	March 26, 1976	086
December 3, 1976	338	April 18, 1977	108
November 21, 1977	325	April 9, 1978	099
December 3, 1978	337	April 16, 1979	106
December 22, 1979	356	April 1, 1980	092
December 4, 1980	339	March 14, 1981	073
November 15, 1981	319	April 10, 1982	100
December 5, 1982	339	May 14, 1983	134
November 17, 1983	321	April 3, 1984	094
December 9, 1984	344	April 23, 1985	113
December 23, 1985	357	April 16, 1986	106
January 2, 1987	002	March 7, 1987	066
December 14, 1987	348	April 5, 1988	096
November 14, 1988	319	April 27, 1989	117
November 18, 1989	322	April 21, 1990	111
November 30, 1990	334	March 2, 1991	061
January 1, 1992	001	April 11, 1992	102
December 4, 1992	339	March 4, 1993	063
December 7, 1993	341	March 22, 1994	081
November 28, 1994	332	April 10, 1995	100
December 1, 1995	335	April 18, 1996	109
December 5, 1996	340	March 13, 1997	072
November 29, 1997	333	March 25, 1998	084
October 30, 1998	303	April 27, 1999	117
October 31, 1999	304	April 29, 2000	120
October 18, 2000	292	April 10, 2001	100
November 26, 2001	330	March 8, 2002	067
December 31, 2002	365	March 14, 2003	073
December 12, 2003	346	March 30, 2004	090
December 8, 2004	343	March 25, 2005	084
November 18, 2005	322	May 4, 2006	124

Table 2 - continued

Onset Day	Julian Day	Demise Day	Julian Day
December 7, 2006	341	April 1, 2007	091
December 10, 2007	344	April 6, 2008	097
November 26, 2008	331	March 18, 2009	077
December 10, 2009	344	April 20, 2010	110
October 8, 2010	281	April 17, 2011	107
November 10, 2011	314	March 30, 2012	090
December 10, 2012	345	April 13, 2013	103
November 18, 2013	322	April 29, 2014	119
November 25, 2014	329	March 29, 2015	088

Table 3: The total rainfall accumulation during each Australian monsoon season (in mm) and the rainfall rate during that season (in mm/day).

Season	Rainfall total	Length of Season	Rain rate per day
1900-1901	246.537	80	3.082
1901-1902	110.123	31	3.552
1902-1903	229.062	85	2.695
1903-1904	353.798	136	2.601
1904-1905	129.308	58	2.229
1905-1906	97.5644	46	2.121
1906-1907	301.118	121	2.489
1907-1908	324.446	108	3.004
1908-1909	179.267	79	2.269
1909-1910	365.741	146	2.505
1910-1911	399.64	166	2.407
1911-1912	274.313	102	2.689
1912-1913	324.396	96	3.379
1913-1914	357.826	111	3.224
1914-1915	251.262	93	2.702
1915-1916	341.519	108	3.162
1916-1917	391.87	130	3.014
1917-1918	390.667	104	3.756
1918-1919	282.535	79	3.576
1919-1920	262.686	88	2.985
1920-1921	449.63	136	3.306
1921-1922	400.101	95	4.212
1922-1923	374.137	122	3.067
1923-1924	300.409	97	3.097
1924-1925	500.063	139	3.597
1925-1926	278.462	88	3.164
1926-1927	412.991	129	3.201
1927-1928	320.694	110	2.915
1928-1929	408.849	109	3.751
1929-1930	342.236	76	4.503
1930-1931	365.614	137	2.669
1931-1932	295.884	94	3.148
1932-1933	353.356	135	2.617
1933-1934	460.556	130	3.543
1934-1935	300.594	87	3.455

Table 3 - continued

Season	Rainfall total	Length of Season	Rain rate per day
1935-1936	304.902	105	2.904
1936-1937	372.631	103	3.618
1937-1938	310.594	73	4.255
1938-1939	455.341	136	3.348
1939-1940	471.074	105	4.486
1940-1941	380.855	99	3.847
1941-1942	262.254	55	4.768
1942-1943	392.668	102	3.850
1943-1944	380.162	103	3.691
1944-1945	438.221	124	3.534
1945-1946	381.339	82	4.650
1946-1947	345.025	105	3.286
1947-1948	336.138	117	2.873
1948-1949	407.591	149	2.735
1949-1950	483.148	129	3.745
1950-1951	461.701	123	3.754
1951-1952	152.835	49	3.119
1952-1953	361.504	115	3.144
1953-1954	401.679	129	3.114
1954-1955	406.358	104	3.907
1955-1956	451.216	123	3.668
1956-1957	499.505	125	3.996
1957-1958	350.552	128	2.739
1958-1959	197.835	139	1.423
1959-1960	398.305	99	4.023
1960-1961	265.196	78	3.400
1961-1962	374.489	81	4.623
1962-1963	476.028	124	3.839
1963-1964	378.845	100	3.788
1964-1965	442.95	143	3.098
1965-1966	385.071	98	3.929
1966-1967	440.152	82	5.368
1967-1968	552.347	158	3.496
1968-1969	432.276	99	4.366
1969-1970	319.439	103	3.101

Table 3 - continued

Season	Rainfall total	Length of Season	Rain rate per day
1970-1971	530.656	151	3.514
1971-1972	499.49	142	3.518
1972-1973	465.4	111	4.193
1973-1974	842.647	156	5.402
1974-1975	510.638	131	3.898
1975-1976	633.225	123	5.148
1976-1977	570.173	136	4.192
1977-1978	452.768	139	3.257
1978-1979	498.047	134	3.717
1979-1980	428.499	101	4.243
1980-1981	494.434	100	4.944
1981-1982	576.59	146	3.949
1982-1983	418.535	160	2.616
1983-1984	580.54	138	4.207
1984-1985	464.635	135	3.442
1985-1986	361.81	114	3.174
1986-1987	367.967	64	5.749
1987-1988	342.369	113	3.030
1988-1989	578.429	164	3.527
1989-1990	349.933	154	2.272
1990-1991	499.131	92	5.425
1991-1992	257.497	101	2.549
1992-1993	463.157	90	5.146
1993-1994	441.214	105	4.202
1994-1995	545.796	133	4.104
1995-1996	492.752	139	3.550
1996-1997	556.939	98	5.683
1997-1998	488.655	116	4.213
1998-1999	740.379	179	4.136
1999-2000	797.033	181	4.403
2000-2001	789.15	174	4.535
2001-2002	377.666	102	3.703
2002-2003	434.831	73	5.957
2003-2004	611.269	109	5.608
2004-2005	379.359	107	3.545

Table 3 - continued

Season	Rainfall total	Length of Season	Rain rate per day
2005-2006	763.146	167	4.570
2006-2007	527.485	115	4.587
2007-2008	542.474	118	4.597
2008-2009	605.663	112	5.408
2009-2010	577.103	131	4.405
2010-2011	973.839	191	5.099
2011-2012	594.899	141	4.219
2012-2013	428.595	124	3.456
2013-2014	633.911	162	3.913
2014-2015	432.691	124	3.489

Table 4: December to February Niño 3.4 sea surface anomalies from 1900 to 2011.

Season	DJF Nino 3.4 SST anomaly
1900-1901	0.142
1901-1902	-0.024
1902-1903	1.597
1903-1904	-1.123
1904-1905	0.980
1905-1906	0.798
1906-1907	-0.686
1907-1908	0.022
1908-1909	-1.497
1909-1910	-1.649
1910-1911	-1.133
1911-1912	1.352
1912-1913	-0.609
1913-1914	0.865
1914-1915	0.961
1915-1916	-0.755
1916-1917	-1.746
1917-1918	-0.725
1918-1919	0.697
1919-1920	0.412
1920-1921	-0.763
1921-1922	-0.541
1922-1923	-1.241
1923-1924	0.587
1924-1925	-1.307
1925-1926	1.223
1926-1927	-0.505
1927-1928	0.190
1928-1929	-0.479
1929-1930	0.332
1930-1931	1.136
1931-1932	-0.623
1932-1933	-0.497
1933-1934	-1.380
1934-1935	-0.402
1935-1936	-0.182
1936-1937	-0.543
1937-1938	-0.462

Table 4 - continued

Season	DJF Nino 3.4 SST anomaly
1938-1939	-1.376
1939-1940	0.812
1940-1941	1.678
1941-1942	0.810
1942-1943	-1.681
1943-1944	-0.471
1944-1945	-0.861
1945-1946	0.067
1946-1947	0.060
1947-1948	-0.107
1948-1949	-0.220
1949-1950	-1.488
1950-1951	-0.867
1951-1952	0.473
1952-1953	0.408
1953-1954	0.632
1954-1955	-0.847
1955-1956	-1.160
1956-1957	-0.322
1957-1958	1.840
1958-1959	0.605
1959-1960	-0.130
1960-1961	0.019
1961-1962	-0.249
1962-1963	-0.450
1963-1964	1.020
1964-1965	-0.591
1965-1966	1.375
1966-1967	-0.203
1967-1968	-0.559
1968-1969	1.191
1969-1970	0.676
1970-1971	-1.128
1971-1972	-0.513
1972-1973	1.968
1973-1974	-1.757
1974-1975	-0.413
1975-1976	-1.430

Table 4 - continued

Season	DJF Nino 3.4 SST anomaly
1976-1977	0.761
1977-1978	0.839
1978-1979	0.063
1979-1980	0.624
1980-1981	-0.153
1981-1982	0.177
1982-1983	2.425
1983-1984	-0.222
1984-1985	-0.761
1985-1986	-0.286
1986-1987	1.415
1987-1988	0.920
1988-1989	-1.546
1989-1990	0.295
1990-1991	0.601
1991-1992	1.923
1992-1993	0.478
1993-1994	0.385
1994-1995	1.362
1995-1996	-0.558
1996-1997	-0.224
1997-1998	2.465
1998-1999	-1.229
1999-2000	-1.422
2000-2001	-0.445
2001-2002	0.098
2002-2003	1.348
2003-2004	0.550
2004-2005	0.840
2005-2006	-0.574
2006-2007	0.954
2007-2008	-1.237
2008-2009	-0.553
2009-2010	1.861
2010-2011	-1.108

Table 5: December to February Niño 3.4 sea surface anomalies from 1900 to 2011 with the trend removed.

Season	DJF Nino 3.4 SST anomoly (no trend)
1900-1901	0.412
1901-1902	0.242
1902-1903	1.859
1903-1904	-0.866
1904-1905	1.231
1905-1906	1.045
1906-1907	-0.444
1907-1908	0.259
1908-1909	-1.265
1909-1910	-1.421
1910-1911	-0.910
1911-1912	1.570
1912-1913	-0.396
1913-1914	1.074
1914-1915	1.165
1915-1916	-0.556
1916-1917	-1.552
1917-1918	-0.536
1918-1919	0.881
1919-1920	0.592
1920-1921	-0.588
1921-1922	-0.371
1922-1923	-1.076
1923-1924	0.747
1924-1925	-1.151
1925-1926	1.374
1926-1927	-0.359
1927-1928	0.331
1928-1929	-0.342
1929-1930	0.464
1930-1931	1.262
1931-1932	-0.501
1932-1933	-0.380
1933-1934	-1.267
1934-1935	-0.295
1935-1936	-0.079
1936-1937	-0.445

Table 5 - continued

Season	DJF Nino 3.4 SST anomoly (no trend)
1937-1938	-0.369
1938-1939	-1.287
1939-1940	0.895
1940-1941	1.756
1941-1942	0.884
1942-1943	-1.612
1943-1944	-0.407
1944-1945	-0.801
1945-1946	0.122
1946-1947	0.110
1947-1948	-0.062
1948-1949	-0.179
1949-1950	-1.452
1950-1951	-0.836
1951-1952	0.499
1952-1953	0.429
1953-1954	0.648
1954-1955	-0.836
1955-1956	-1.153
1956-1957	-0.320
1957-1958	1.837
1958-1959	0.597
1959-1960	-0.143
1960-1961	0.002
1961-1962	-0.271
1962-1963	-0.476
1963-1964	0.989
1964-1965	-0.628
1965-1966	1.334
1966-1967	-0.249
1967-1968	-0.610
1968-1969	1.136
1969-1970	0.616
1970-1971	-1.193
1971-1972	-0.583
1972-1973	1.894
1973-1974	-1.837
1974-1975	-0.498

Table 5 - continued

Season	DJF Nino 3.4 SST anomoly (no trend)
1975-1976	-1.520
1976-1977	0.667
1977-1978	0.741
1978-1979	-0.041
1979-1980	0.515
1980-1981	-0.266
1981-1982	0.059
1982-1983	2.302
1983-1984	-0.350
1984-1985	-0.893
1985-1986	-0.424
1986-1987	1.273
1987-1988	0.773
1988-1989	-1.697
1989-1990	0.139
1990-1991	0.439
1991-1992	1.757
1992-1993	0.307
1993-1994	0.209
1994-1995	1.182
1995-1996	-0.744
1996-1997	-0.415
1997-1998	2.271
1998-1999	-1.429
1999-2000	-1.626
2000-2001	-0.654
2001-2002	-0.116
2002-2003	1.129
2003-2004	0.327
2004-2005	0.611
2005-2006	-0.807
2006-2007	0.716
2007-2008	-1.480
2008-2009	-0.801
2009-2010	1.609
2010-2011	-1.365

Table 6: The December to February area averaged rainfall accumulation for each year from 1900-2011 (in mm) as well as the detrended DJF rainfall accumulation. Also included is the total monsoon season accumulated rainfall for each monsoon season from 1900-2011 (in mm) as well as the detrended data.

Season	DJF Rainfall Accumulation	DJF Rainfall Accumulation (no trend)	Seasonal Rainfall	Seasonal rainfall (no trend)
1900-1901	170.109	-38.3284	246.537	-8.9902
1901-1902	148.347	-61.9978	110.123	-148.3714
1902-1903	173.292	-38.9602	229.062	-32.3996
1903-1904	256.987	42.8274	353.798	89.3692
1904-1905	153.281	-62.786	129.308	-138.088
1905-1906	120.71	-97.2644	97.5644	-172.7988
1906-1907	236.011	16.1292	301.118	27.7876
1907-1908	259.19	37.4008	324.446	48.1484
1908-1909	155.717	-67.9796	179.267	-99.9978
1909-1910	245.122	19.518	365.741	83.509
1910-1911	255.77	28.2586	399.64	114.4408
1911-1912	189.114	-40.3048	274.313	-13.8534
1912-1913	249.292	17.9658	324.396	33.2624
1913-1914	281.665	48.4314	357.826	63.7252
1914-1915	238.421	3.28	251.262	-45.806
1915-1916	281.381	44.3326	341.519	41.4838
1916-1917	299.819	60.8632	391.87	88.8676
1917-1918	359.523	118.6598	390.667	84.6974
1918-1919	267.787	25.0164	282.535	-26.4018
1919-1920	250.297	5.619	262.686	-49.218
1920-1921	297.021	50.4356	449.63	134.7588
1921-1922	302.414	53.9212	400.101	82.2626
1922-1923	242.673	-7.7272	374.137	53.3314
1923-1924	254.247	1.9394	300.409	-23.3638
1924-1925	332.477	78.262	500.063	173.323
1925-1926	233.219	-22.9034	278.462	-51.2452
1926-1927	326.223	68.1932	412.991	80.3166
1927-1928	209.25	-50.6872	320.694	-14.9476
1928-1929	316.89	55.0454	408.849	70.2402
1929-1930	326.539	62.787	342.236	0.66
1930-1931	253.673	-11.9864	365.614	21.0708
1931-1932	230.424	-37.1428	295.884	-51.6264
1932-1933	240.191	-29.2832	353.356	2.8784

Table 6 - continued

Season	DJF Rainfall Accumulation	DJF Rainfall Accumulation (no trend)	Seasonal Rainfall	Seasonal rainfall (no trend)
1933-1934	326.805	55.4234	460.556	107.1112
1934-1935	179.041	-94.248	300.594	-55.818
1935-1936	213.73	-61.4664	304.902	-54.4772
1936-1937	298.678	21.5742	372.631	10.2846
1937-1938	322.641	43.6298	310.594	-54.7196
1938-1939	325.279	44.3604	455.341	87.0602
1939-1940	370.67	87.844	471.074	99.826
1940-1941	261.836	-22.8974	380.855	6.6398
1941-1942	291.144	4.5032	262.254	-114.9284
1942-1943	314.857	26.3088	392.668	12.5184
1943-1944	280.33	-10.1256	380.162	-2.9548
1944-1945	294.913	2.55	438.221	52.137
1945-1946	381.838	87.5676	381.339	-7.7122
1946-1947	229.768	-66.4098	345.025	-46.9934
1947-1948	233.875	-64.2102	336.138	-58.8476
1948-1949	259.604	-40.3886	407.591	9.6382
1949-1950	371.558	69.658	483.148	82.228
1950-1951	383.37	79.5626	461.701	57.8138
1951-1952	187.183	-118.5318	152.835	-254.0194
1952-1953	276.214	-31.4082	361.504	-48.3176
1953-1954	282.254	-27.2756	401.679	-11.1098
1954-1955	322.669	11.232	406.358	-9.398
1955-1956	327.372	14.0276	451.216	32.4928
1956-1957	347.455	32.2032	499.505	77.8146
1957-1958	260.777	-56.3822	350.552	-74.1056
1958-1959	51.0912	-267.9754	197.835	-229.7898
1959-1960	319.973	-1.001	398.305	-32.287
1960-1961	252.426	-70.4554	265.196	-168.3632
1961-1962	371.224	46.4352	374.489	-62.0374
1962-1963	347.579	20.8828	476.028	36.5344
1963-1964	263.016	-65.5876	378.845	-63.6158
1964-1965	232.248	-98.263	442.95	-2.478
1965-1966	363.309	30.8906	385.071	-63.3242
1966-1967	377.476	43.1502	440.152	-11.2104
1967-1968	409.553	73.3198	552.347	98.0174
1968-1969	352.8	14.6594	432.276	-25.0208

Table 6 - continued

Season	DJF Rainfall Accumulation	DJF Rainfall Accumulation (no trend)	Seasonal Rainfall	Seasonal rainfall (no trend)
1969-1970	248.375	-91.673	319.439	-140.825
1970-1971	276.36	-65.5954	530.656	67.4248
1971-1972	319.585	-24.2778	499.49	33.2916
1972-1973	300.369	-45.4012	465.4	-3.7656
1973-1974	541.426	193.7484	842.647	370.5142
1974-1975	352.605	3.02	510.638	35.538
1975-1976	491.151	139.6586	633.225	155.1578
1976-1977	372.632	19.2322	570.173	89.1386
1977-1978	347.597	-7.7102	452.768	-31.2336
1978-1979	372.369	15.1544	498.047	11.0782
1979-1980	352.797	-6.325	428.499	-61.437
1980-1981	455.78	94.7506	494.434	1.5308
1981-1982	380.485	17.5482	576.59	80.7196
1982-1983	170.414	-194.4302	418.535	-80.3026
1983-1984	413.325	46.5734	580.54	78.7352
1984-1985	285.143	-83.516	464.635	-40.137
1985-1986	304.092	-66.4744	361.81	-145.9292
1986-1987	387.373	14.8992	367.967	-142.7394
1987-1988	246.483	-127.8982	342.369	-171.3046
1988-1989	297.53	-78.7586	578.429	61.7882
1989-1990	205.535	-172.661	349.933	-169.675
1990-1991	496.059	115.9556	499.131	-23.4442
1991-1992	219.059	-162.9518	257.497	-268.0454
1992-1993	461.264	77.3458	463.157	-65.3526
1993-1994	355.451	-30.3746	441.214	-90.2628
1994-1995	379.763	-7.97	545.796	11.352
1995-1996	309.414	-80.2264	492.752	-44.6592
1996-1997	495.322	103.7742	556.939	16.5606
1997-1998	402.23	8.7748	488.655	-54.6906
1998-1999	448.632	53.2694	740.379	194.0662
1999-2000	446.605	49.335	797.033	247.753
2000-2001	535.909	136.7316	789.15	236.9028
2001-2002	342.157	-58.9278	377.666	-177.5484
2002-2003	394.984	-8.0082	434.831	-123.3506
2003-2004	486.038	81.1384	611.269	50.1202
2004-2005	280.746	-126.061	379.359	-184.757

Table 6 - continued

Season	DJF Rainfall Accumulation	DJF Rainfall Accumulation (no trend)	Seasonal Rainfall	Seasonal rainfall (no trend)
2005-2006	390.683	-18.0314	763.146	196.0628
2006-2007	340.983	-69.6388	527.485	-42.5654
2007-2008	448.376	35.8468	542.474	-30.5436
2008-2009	554.336	139.8994	605.663	29.6782
2009-2010	443.625	27.281	577.103	-1.849
2010-2011	586.366	168.1146	973.839	391.9198

APPENDIX B

FIGURES

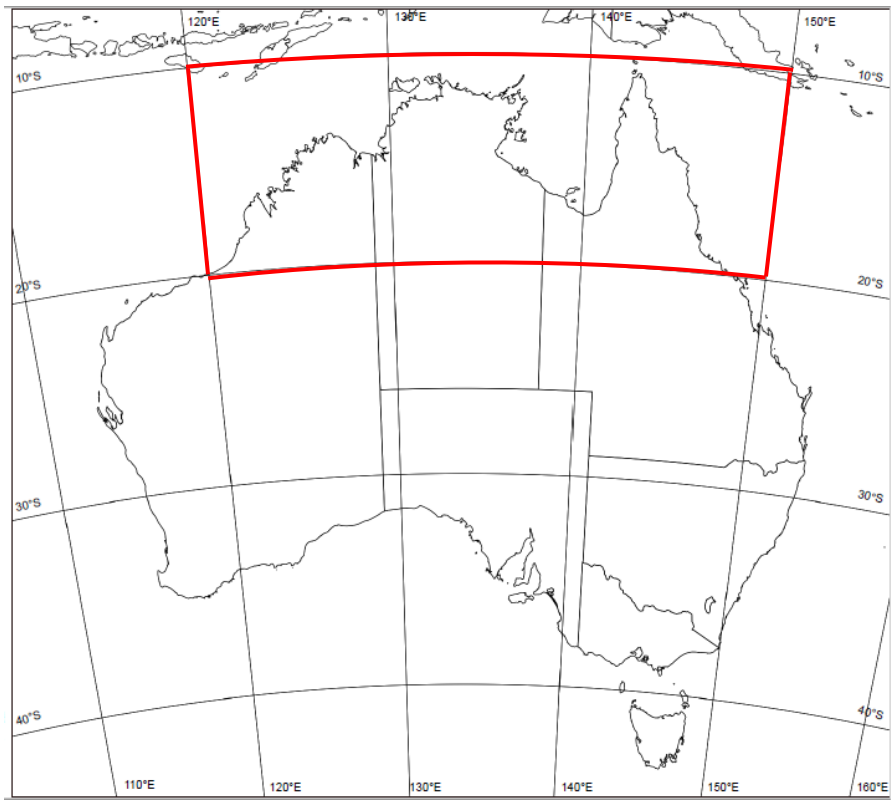

Figure 1: The northern Australian region (outlined by the red box) used to define the Australian Monsoon Rainfall Index (AUSMRI).

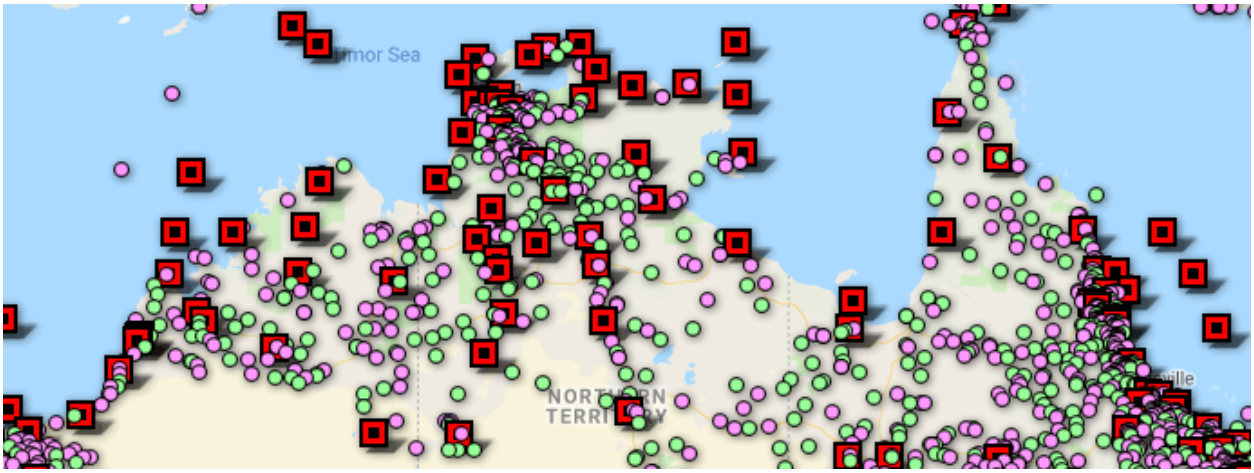

Figure 2: The current map of the rain gauge distribution in Australia, per the Australian Bureau of Meteorology. Green are active rain stations, red are active weather stations, and purple are former rain stations. Sourced from: http://www.australianweathernews.com/sitepages/data/StationMapAustralia.shtml

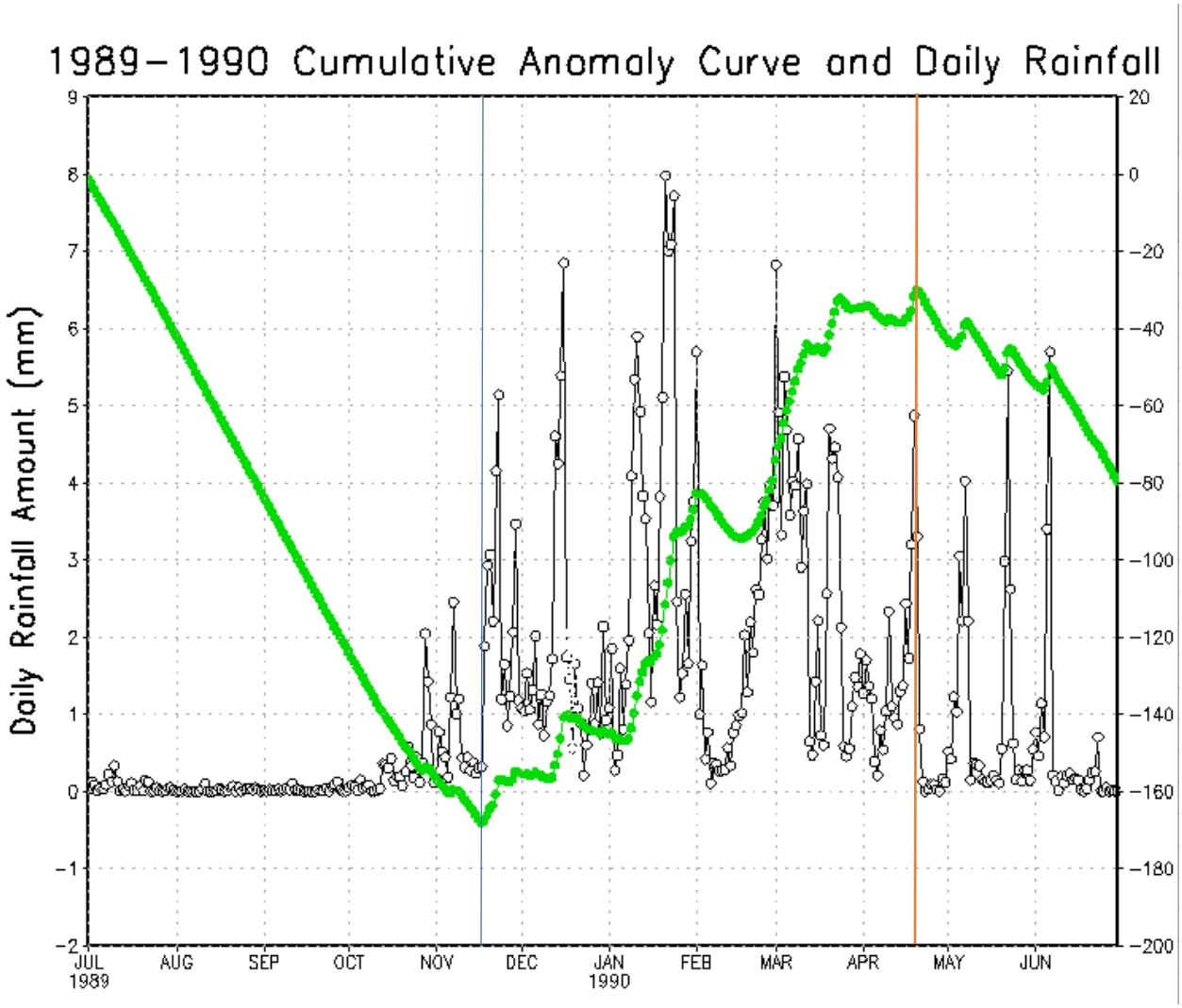

Figure 3: The time series of daily rainfall averaged over northern Australia (black solid line with open circles) overlaid with the corresponding cumulative anomaly curve (green filled circles). The minimum in the cumulative anomaly curve is diagnosed as onset and maximum as demise date of the Australian monsoon for the year 1990. The onset date (November 18th) is marked by the blue line, and the demise date (April 21st) is marked by the orange line.

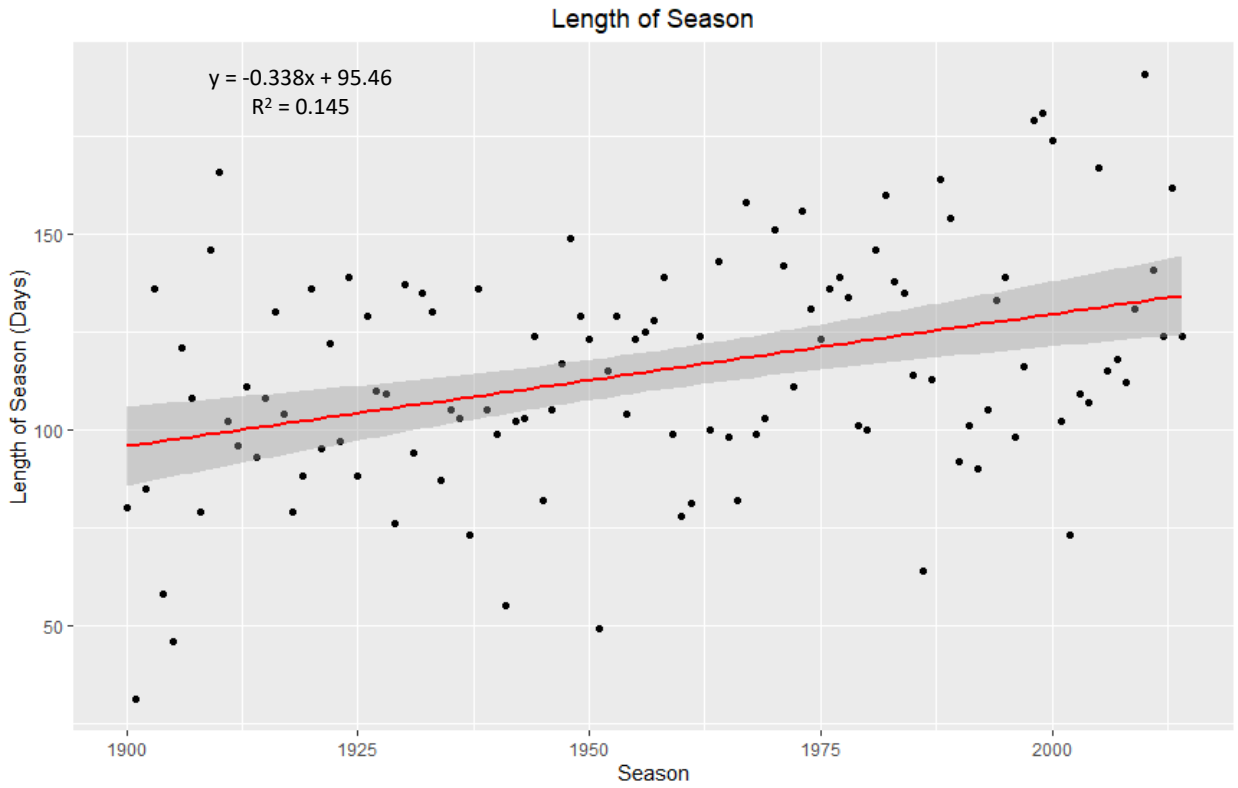

Figure 4: Length of season by year, including a trendline (by least squares fit) to show how the length of the monsoon season has changed over time. The linear regression passes the Mann Kendall test at 99% significance level. The slope of the regression line is indicated in the figure as days/year. The 95% confidence interval for the regression line is shaded.

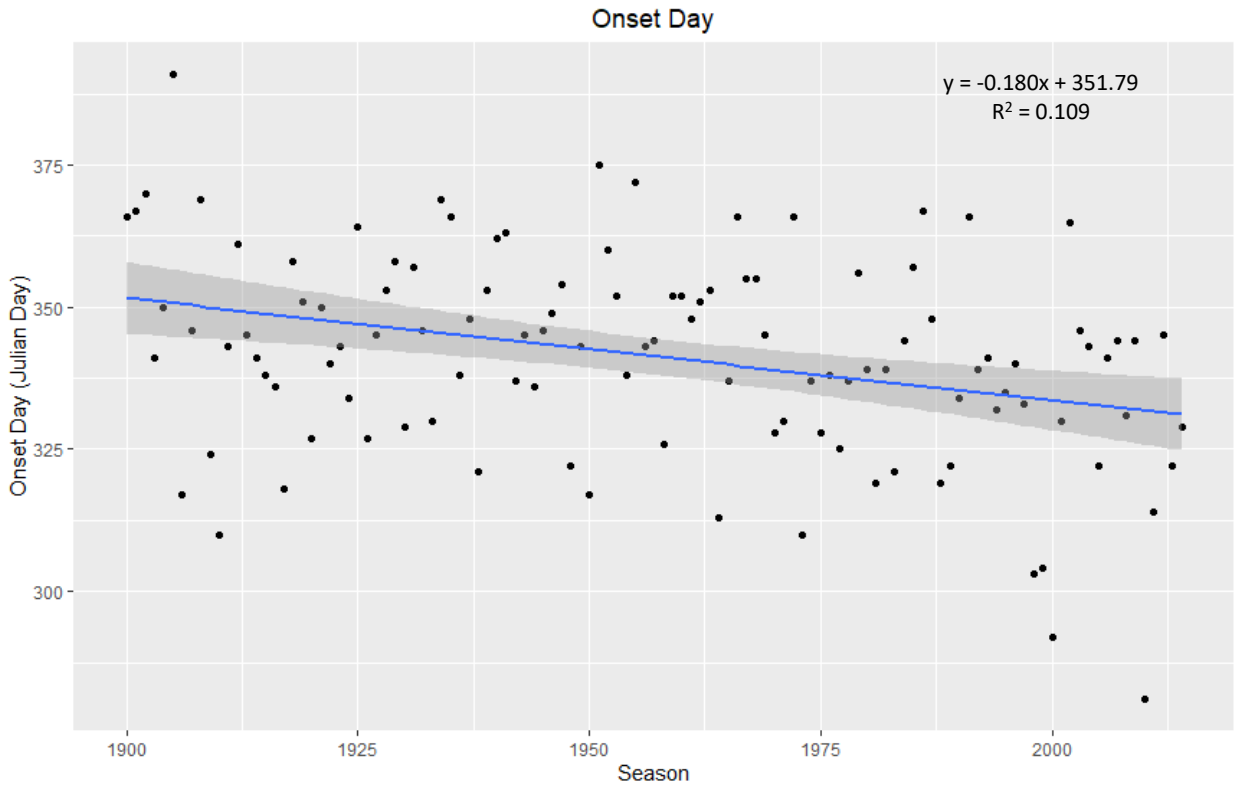

Figure 5: Onset day of each Australian monsoon in Julian Days, note that values larger than 365 (366 during leap years) are onsets occurring in the beginning of the ensuing year. The linear regression passes the Mann Kendall test at 99% significance level. The slope of the regression line is indicated in the figure as Julian day/year. The 95% confidence interval for the regression line is shaded.

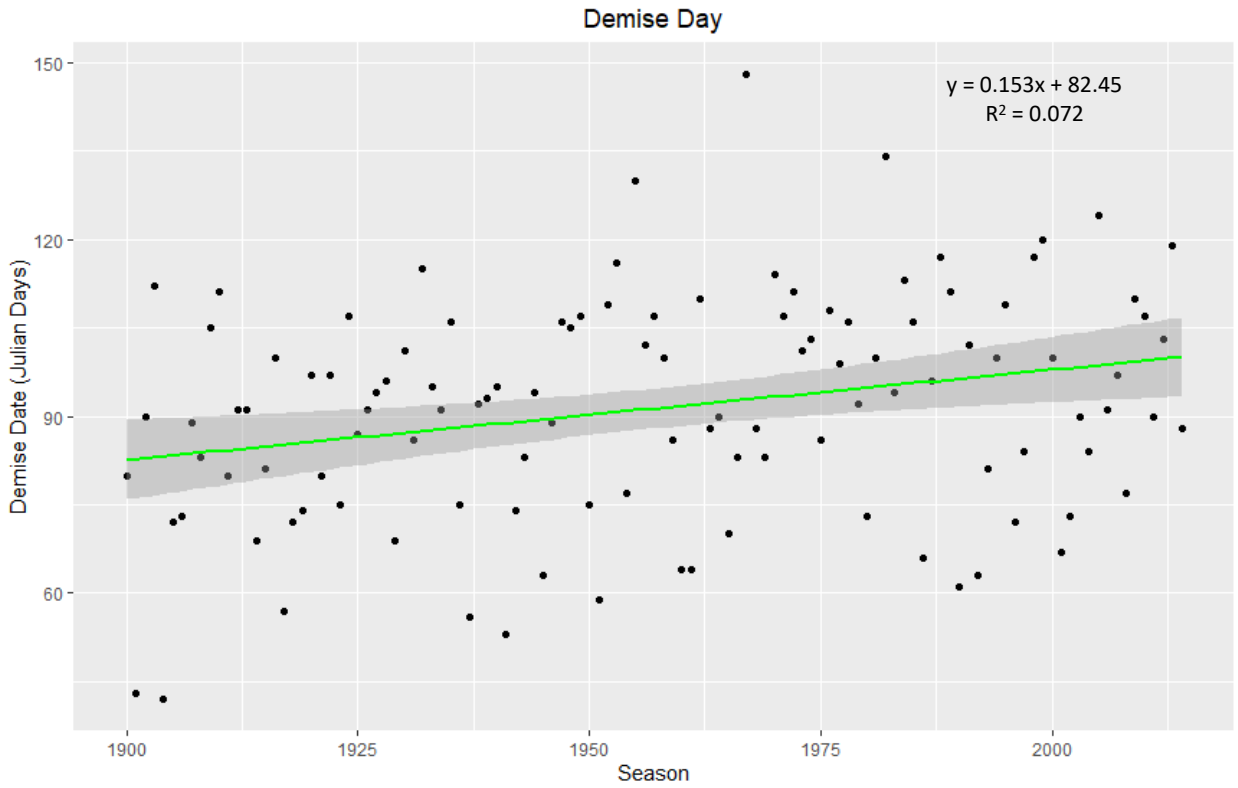

Figure 6: Demise date of the Australian monsoon by year in Julian days. The linear regression passes the Mann Kendall test at 99% significance level. The slope of the regression line is indicated in the figure as Julian day/year. The 95% confidence interval for the regression line is shaded.

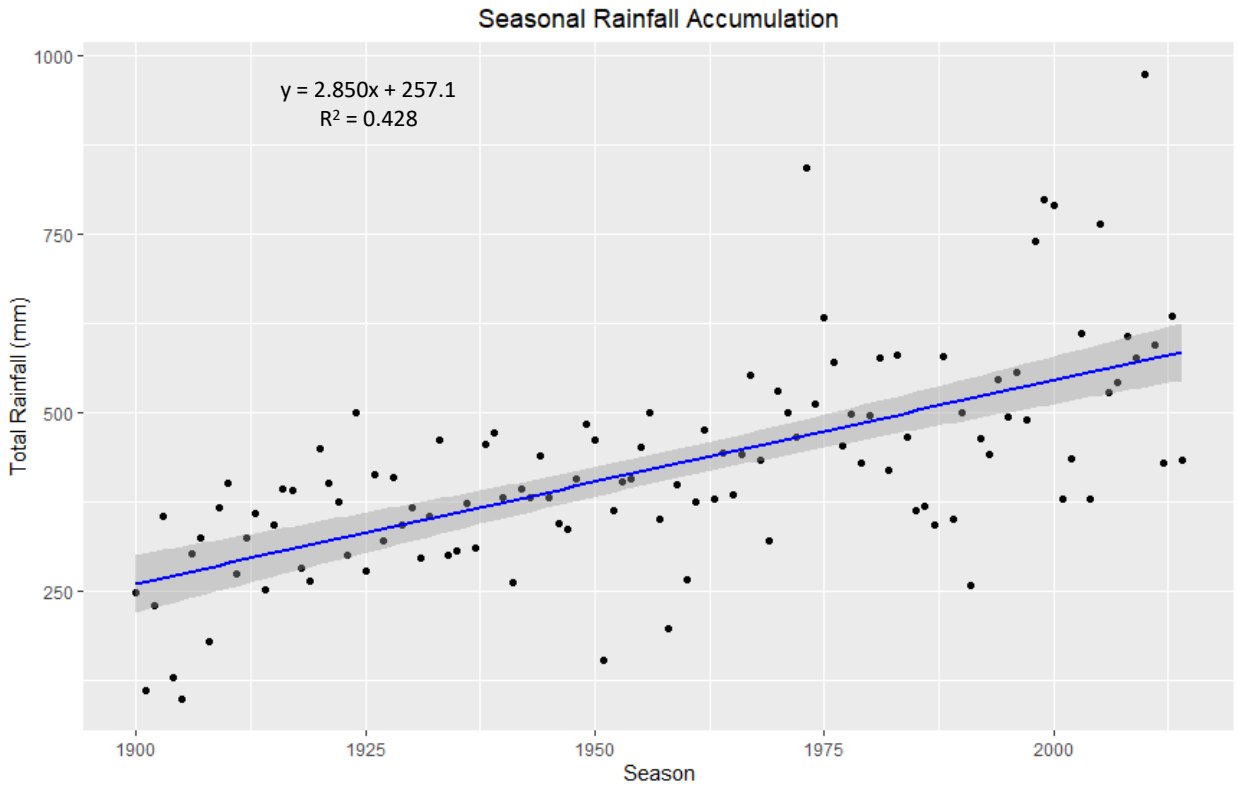

Figure 7: Total seasonal rainfall accumulation during each monsoon season from 1900-2015. The linear regression passes the Mann Kendall test at 99% significance level. The slope of the regression line is indicated in the figure as mm/year. The 95% confidence interval for the regression line is shaded.

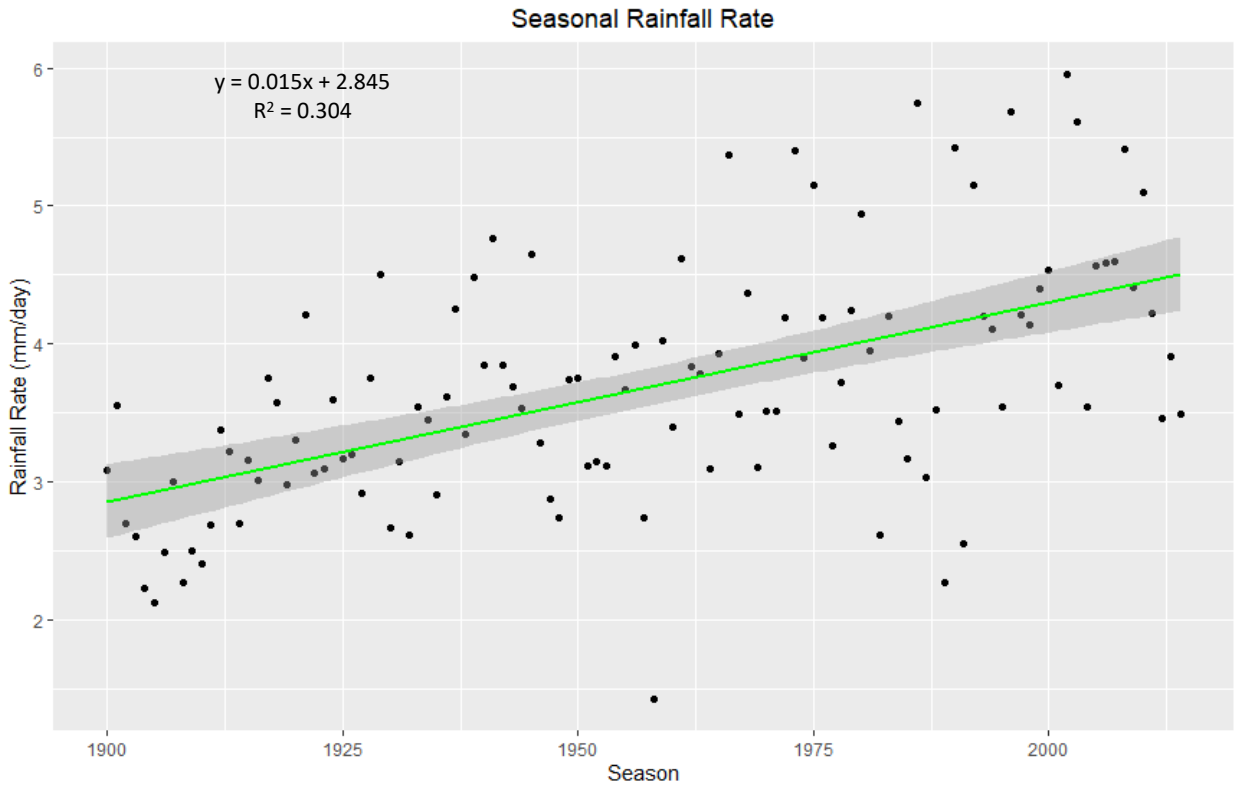

Figure 8: Rainfall rate (in mm/day) for each Australian monsoon season from 1900-2015. The linear regression passes the Mann Kendall test at 99% significance level. The slope of the regression line is indicated in the figure as mm/day/year. The 95% confidence interval for the regression line is shaded.

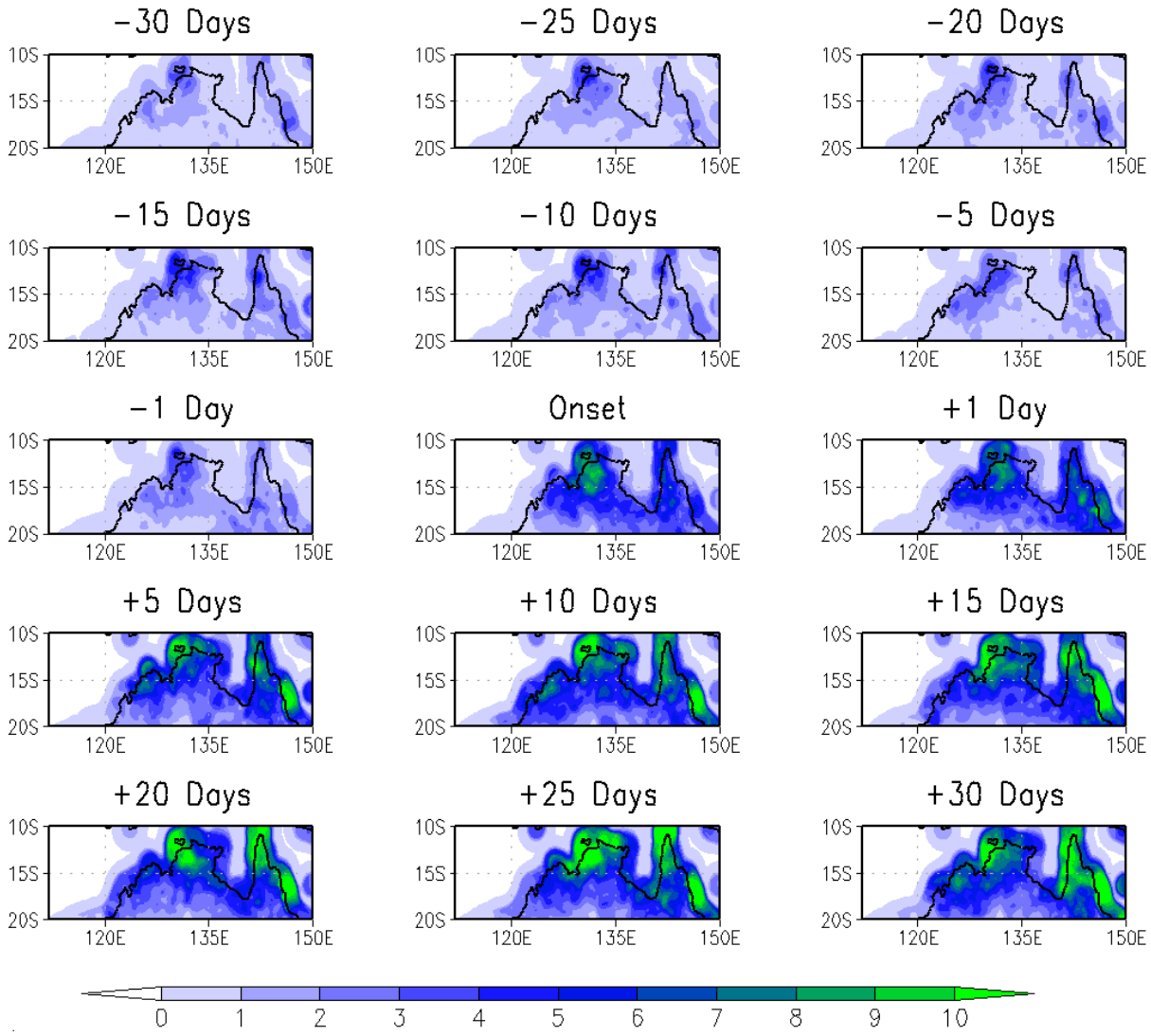

Figure 9: Composite spatial distribution of rainfall (mm/day) over northern Australia (in mm) for 30 days, 25 days, 20 days, 15 days, 10 days, 5 days, 1 day, and for the day of the onset of the northern Australian monsoon as well as the composite spatial distribution of rainfall for 1 day, 5 days, 10 days, 15 days, 20 days, 25 days, and 30 days after the onset of the monsoon over the period from 1900 to 2015.

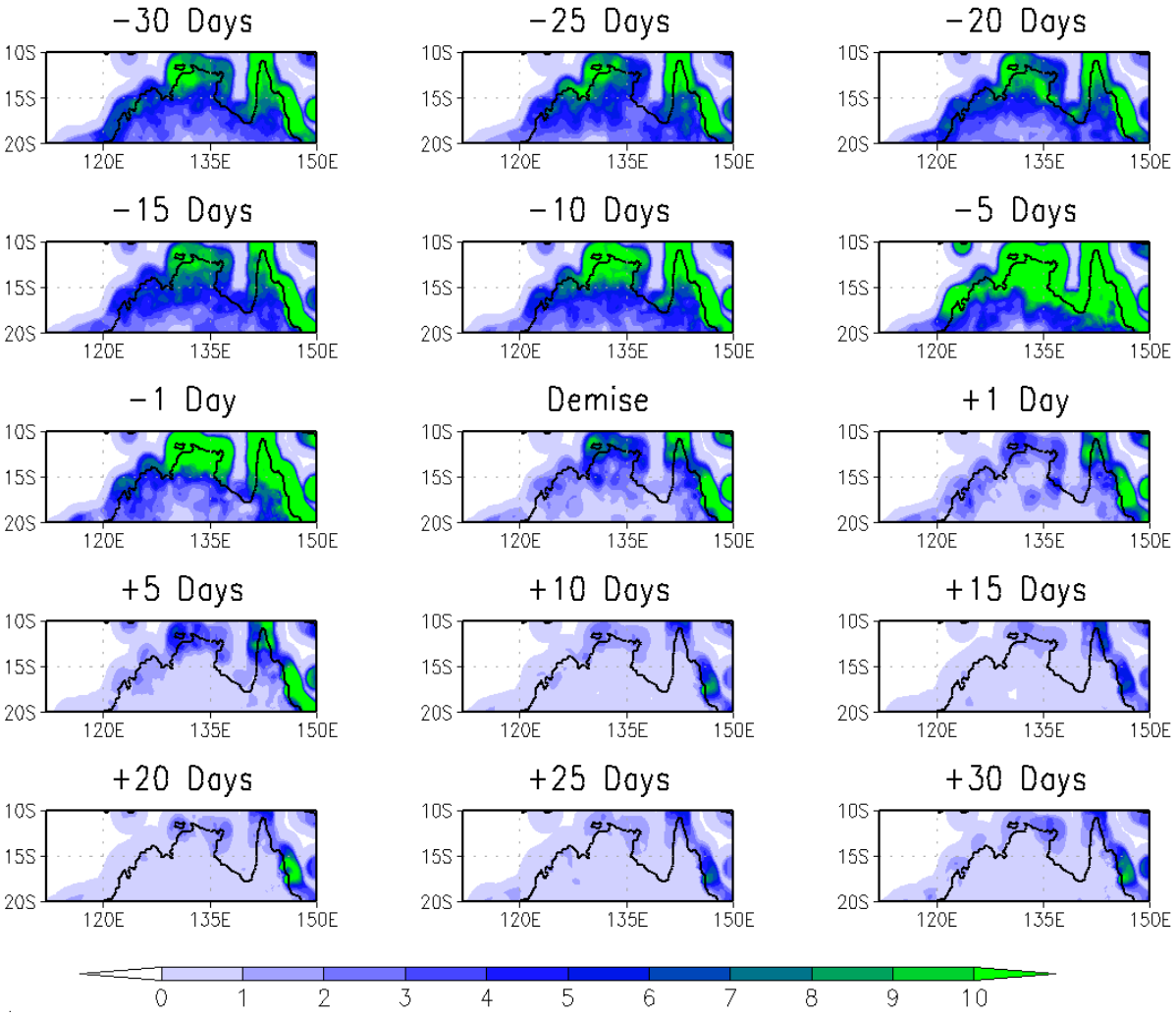

Figure 10: Composite spatial distribution of rainfall (mm/day) over northern Australia (in mm) for 30 days, 25 days, 20 days, 15 days, 10 days, 5 days, 1 day, and for the day of the demise of the northern Australian monsoon as well as the average spatial distribution of rainfall for 1 day, 5 days, 10 days, 15 days, 20 days, 25 days, and 30 days after the demise of the monsoon over the period from 1900 to 2015.

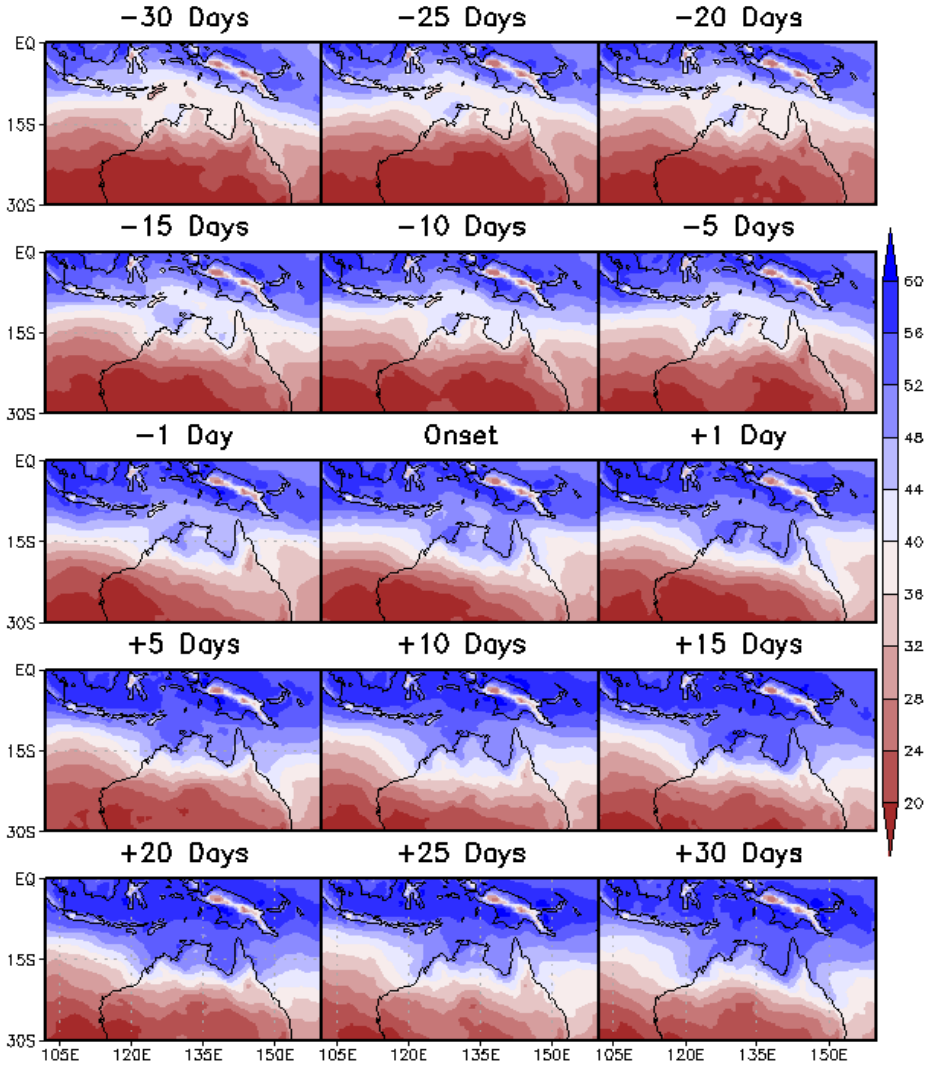

Figure 11: Composite spatial distribution of precipitable water (mm) over the Australia region for 30 days, 25 days, 20 days, 15 days, 10 days, 5 days, 1 day, and for the day of the onset of the northern Australian monsoon as well as the composite spatial distribution of precipitable water for 1 day, 5 days, 10 days, 15 days, 20 days, 25 days, and 30 days after the onset of the monsoon over the period from 1980 to 2010.

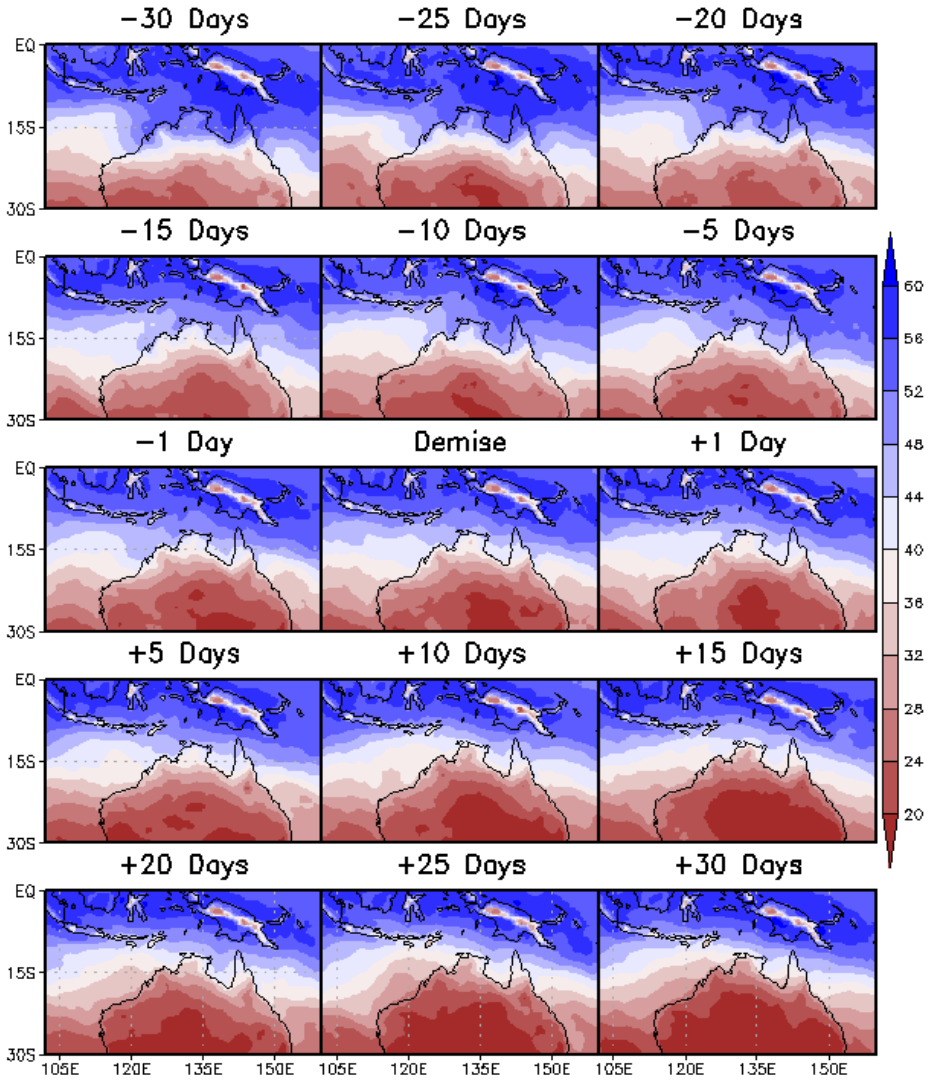

Figure 12: Composite spatial distribution of precipitable water (mm) over the Australian region for 30 days, 25 days, 20 days, 15 days, 10 days, 5 days, 1 day, and for the day of the demise of the northern Australian monsoon as well as the composite spatial distribution of precipitable water for 1 day, 5 days, 10 days, 15 days, 20 days, 25 days, and 30 days after the demise of the monsoon over the period from 1980 to 2010.

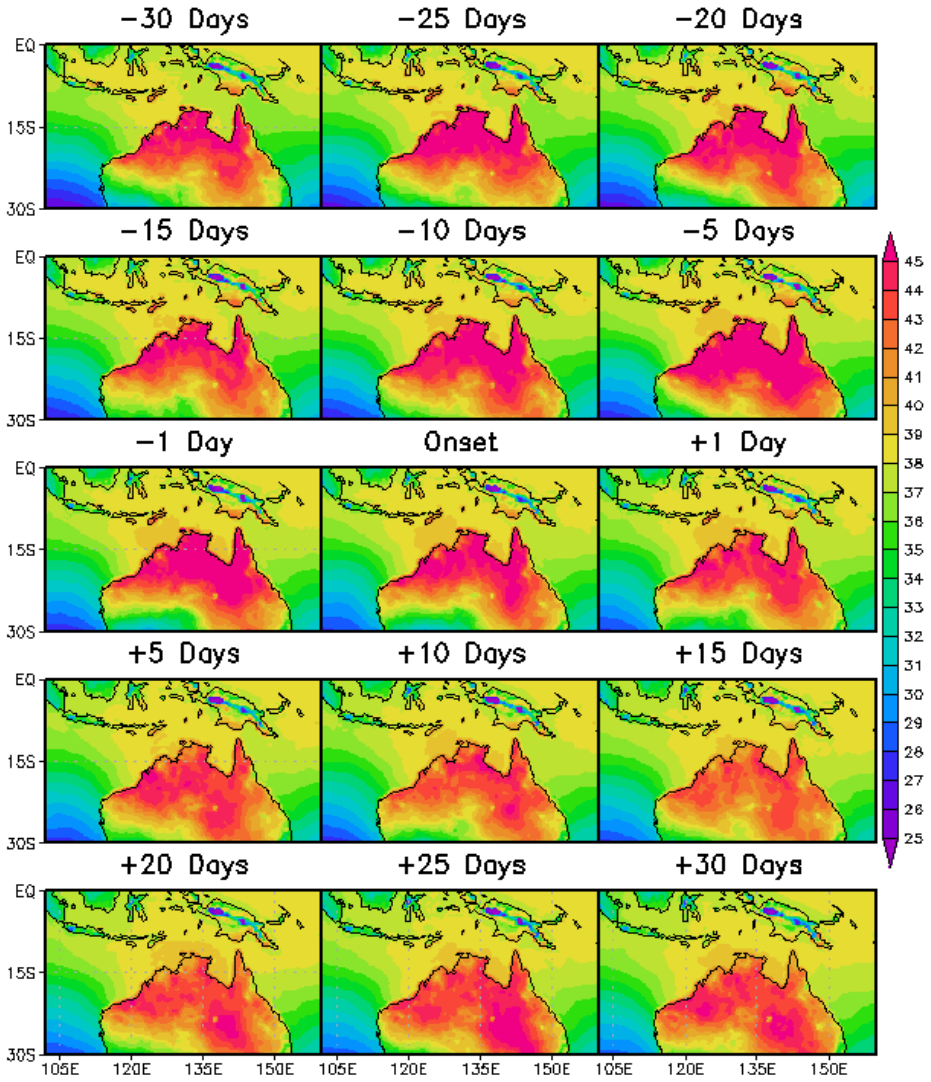

Figure 13: Composite spatial distribution of two meter surface temperature (°C) over the Australian region for 30 days, 25 days, 20 days, 15 days, 10 days, 5 days, 1 day, and for the day of the onset of the northern Australian monsoon as well as the composite spatial distribution of two meter surface temperature for 1 day, 5 days, 10 days, 15 days, 20 days, 25 days, and 30 days after the onset of the monsoon over the period from 1980 to 2010.

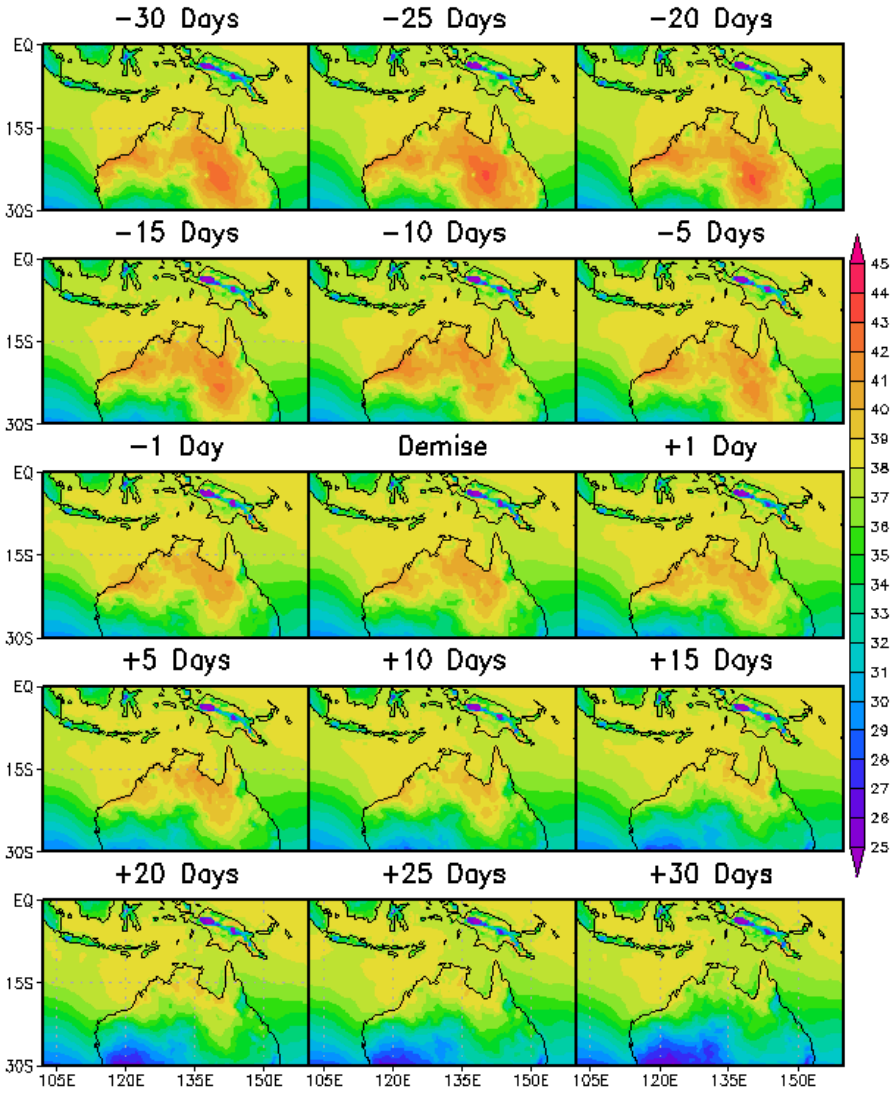

Figure 14: Composite spatial distribution of two-meter surface temperature (°C) for 30 days, 25 days, 20 days, 15 days, 10 days, 5 days, 1 day, and for the day of the demise of the northern Australian monsoon as well as the composite spatial distribution of two-meter surface temperature for 1 day, 5 days, 10 days, 15 days, 20 days, 25 days, and 30 days after the demise of the monsoon over the period from 1980 to 2010.

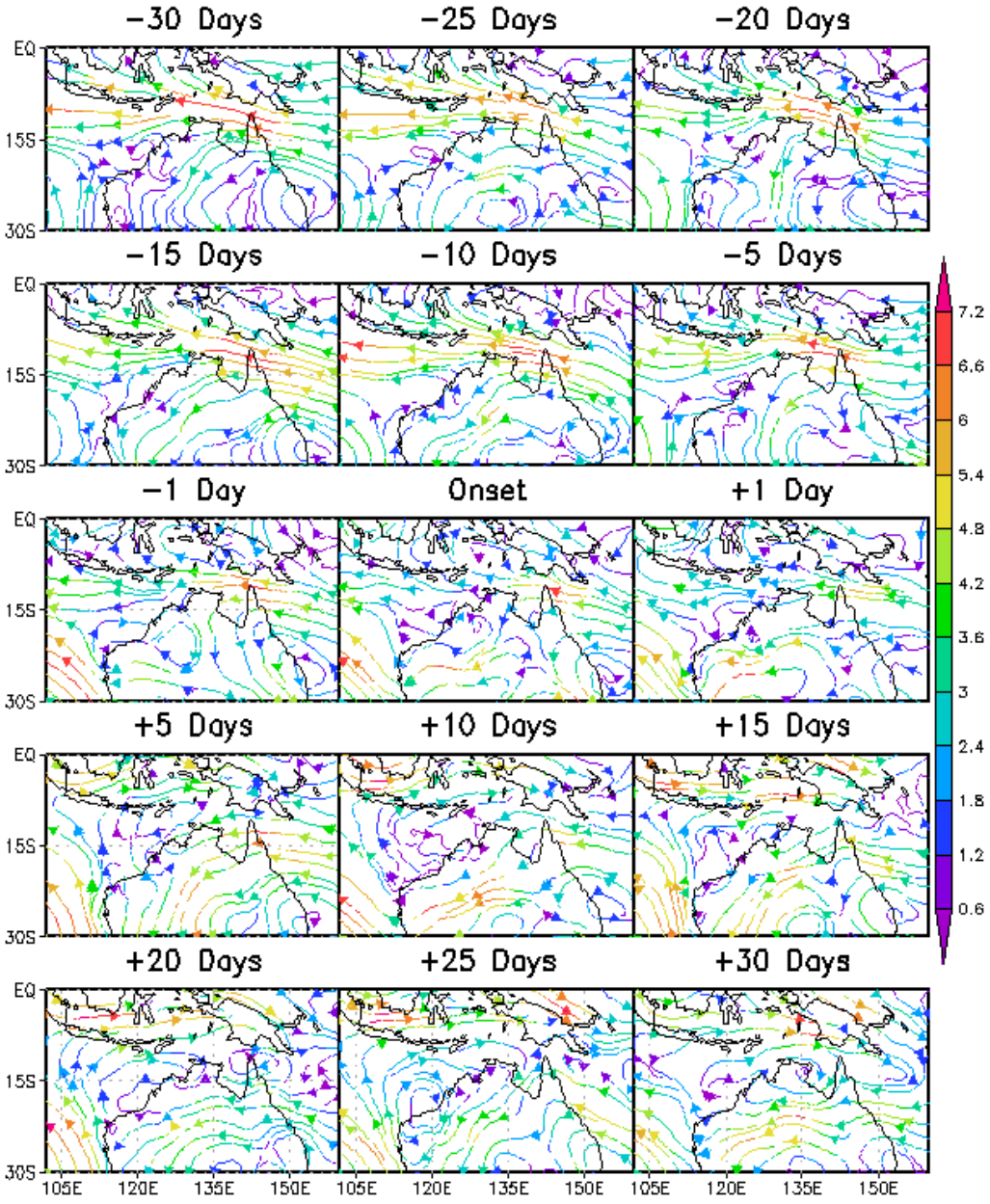

Figure 15: Composite of 850mb winds (m/s) over the Australian region for 30 days, 25 days, 20 days, 15 days, 10 days, 5 days, 1 day, and for the day of the onset of the northern Australian monsoon as well as the composite of 850mb winds for 1 day, 5 days, 10 days, 15 days, 20 days, 25 days, and 30 days after the onset of the monsoon over the period from 1980 to 2010.

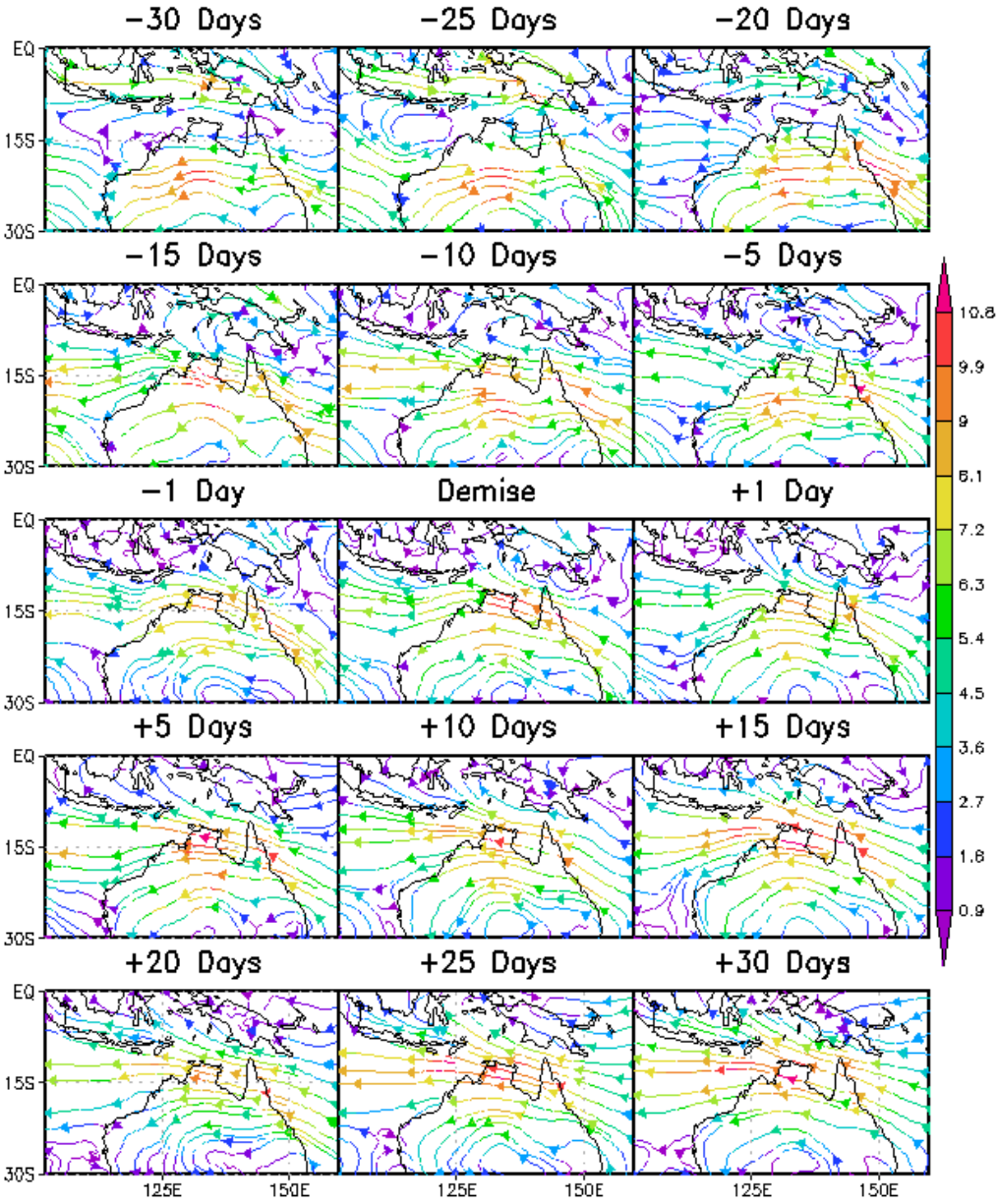

Figure 16: Composite of 850mb winds (m/s) over the Australian region for 30 days, 25 days, 20 days, 15 days, 10 days, 5 days, 1 day, and for the day of the demise of the northern Australian monsoon as well as the composite of 850mb winds for 1 day, 5 days, 10 days, 15 days, 20 days, 25 days, and 30 days after the demise of the monsoon over the period from 1980 to 2010.

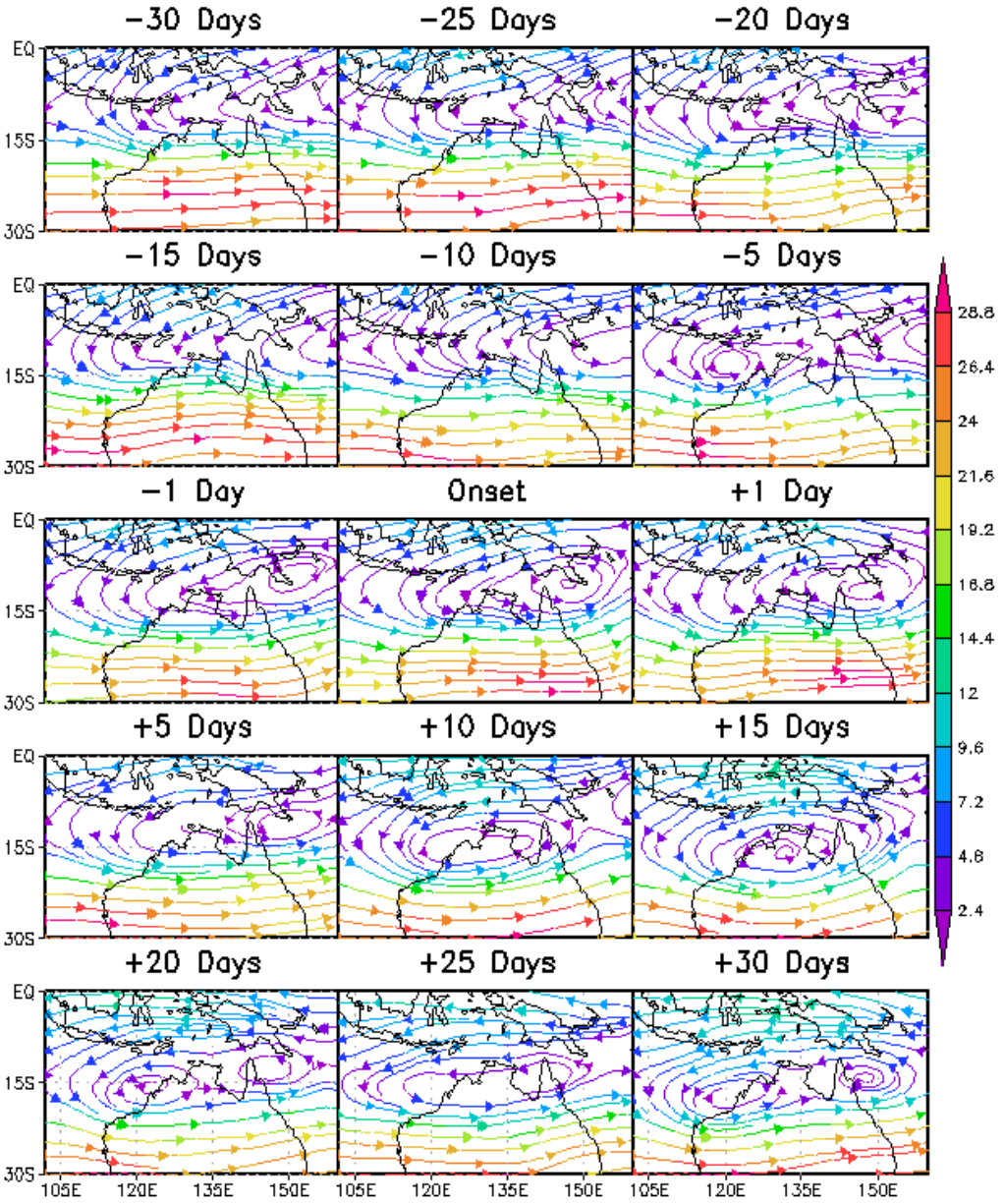

Figure 17: Composite of 200mb winds (m/s) over the Australian region for 30 days, 25 days, 20 days, 15 days, 10 days, 5 days, 1 day, and for the day of the onset of the northern Australian monsoon as well as the composite of 200mb winds for 1 day, 5 days, 10 days, 15 days, 20 days, 25 days, and 30 days after the onset of the monsoon over the period from 1980 to 2010.

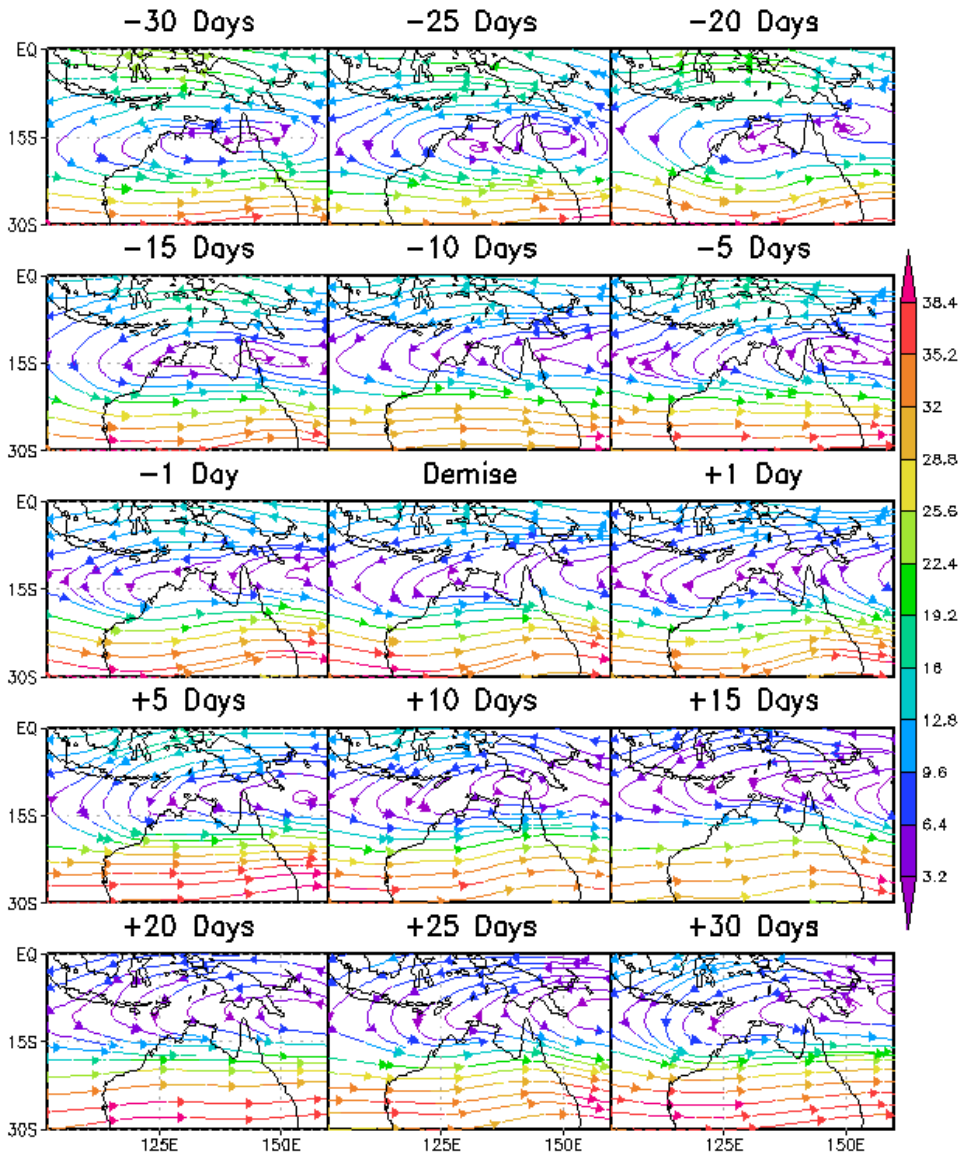

Figure 18: Composite of 200mb winds (m/s) over the Australian region for 30 days, 25 days, 20 days, 15 days, 10 days, 5 days, 1 day, and for the day of the demise of the northern Australian monsoon as well as the composite of 200mb winds for 1 day, 5 days, 10 days, 15 days, 20 days, 25 days, and 30 days after the demise of the monsoon over the period from 1980 to 2010.

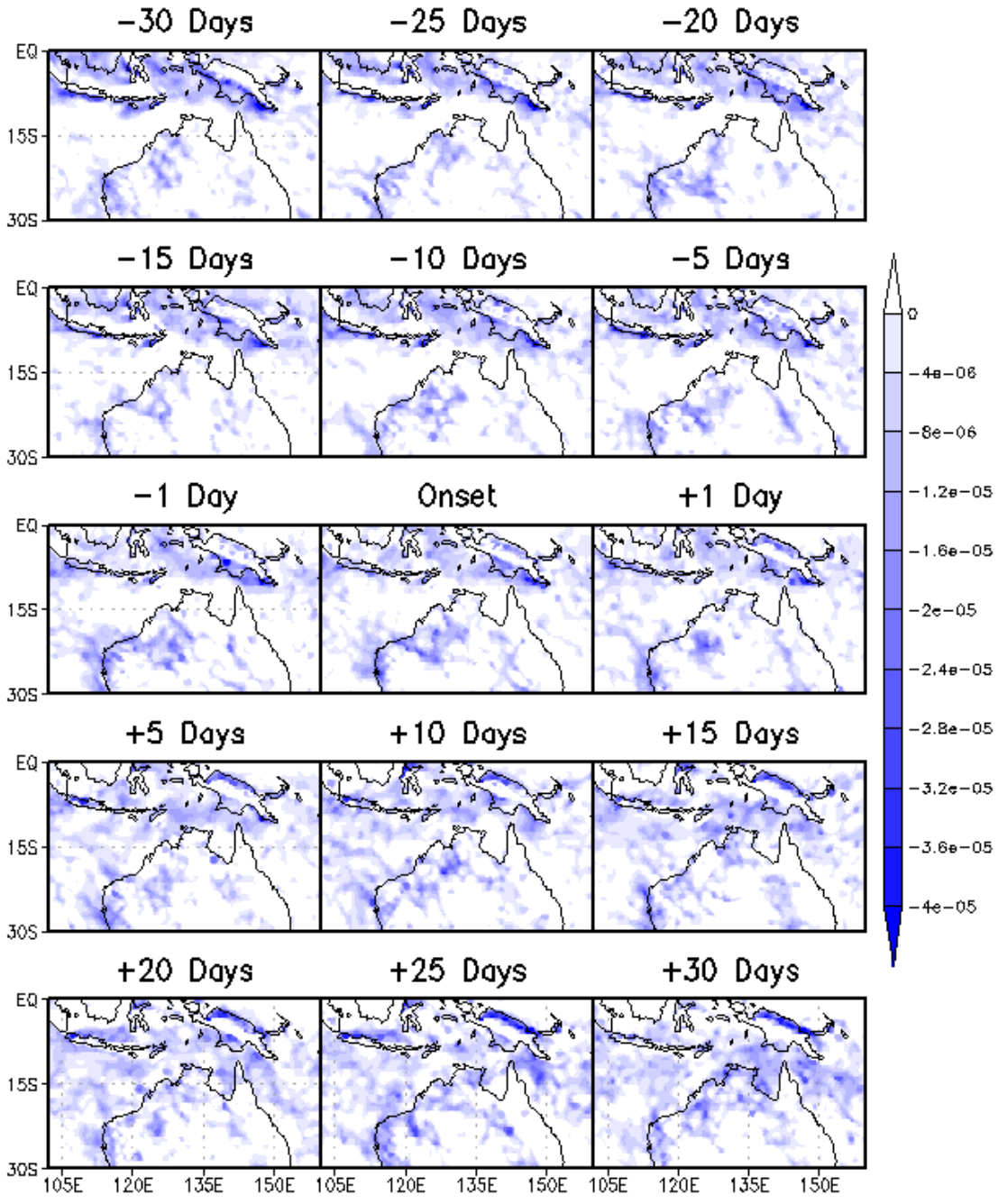

Figure 19: Composite of 850mb vorticity (s^{-1}) over the Australian region for 30 days, 25 days, 20 days, 15 days, 10 days, 5 days, 1 day, and for the day of the onset of the northern Australian monsoon as well as the composite of 850mb vorticity for 1 day, 5 days, 10 days, 15 days, 20 days, 25 days, and 30 days after the onset of the monsoon over the period from 1980 to 2010. Only areas of cyclonic vorticity are shaded.

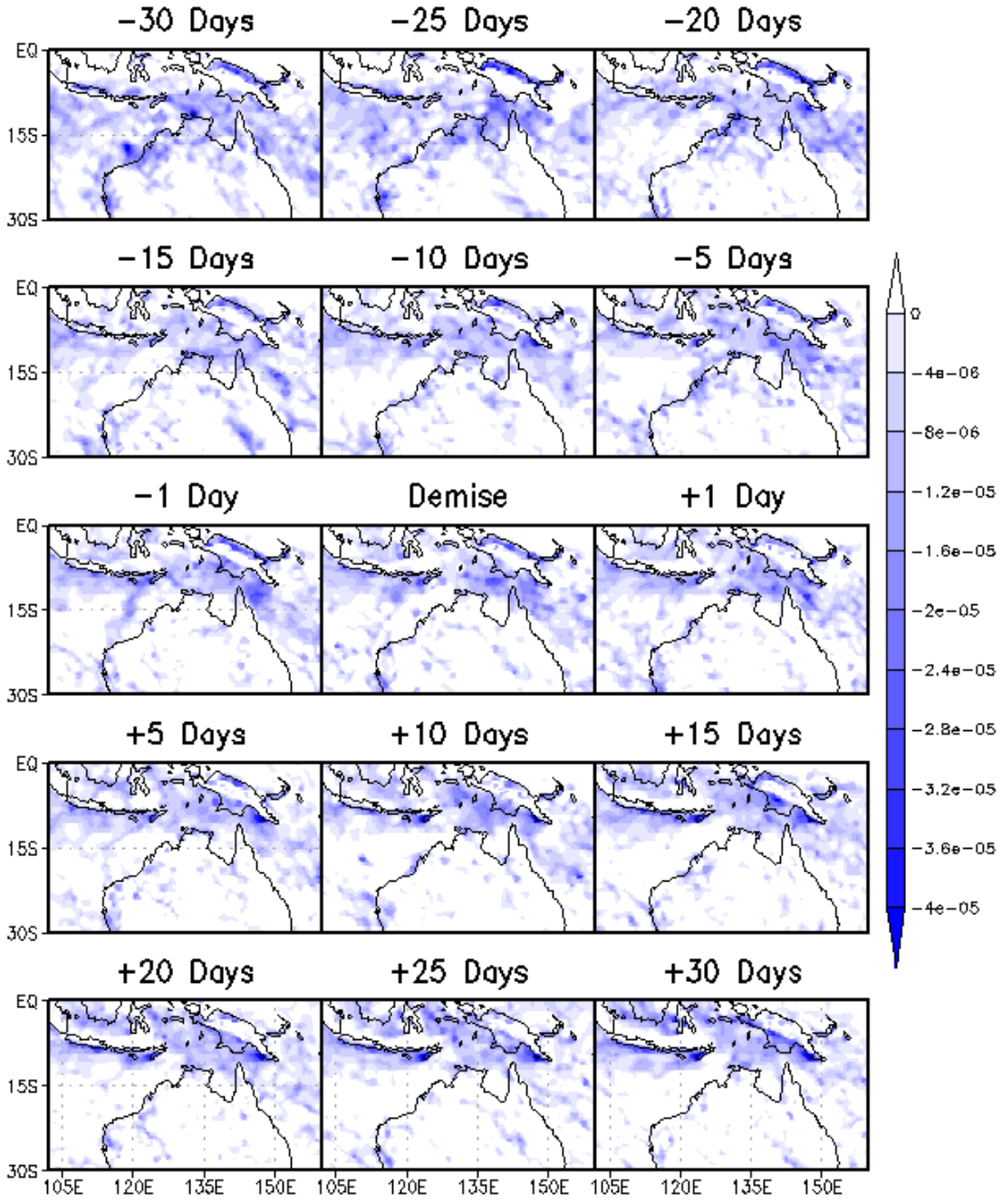

Figure 20: Composite of 850mb vorticity (s^{-1}) over the Australian region for 30 days, 25 days, 20 days, 15 days, 10 days, 5 days, 1 day, and for the day of the demise of the northern Australian monsoon as well as the composite of 850mb vorticity for 1 day, 5 days, 10 days, 15 days, 20 days, 25 days, and 30 days after the demise of the monsoon over the period from 1980 to 2010. Only areas of cyclonic vorticity are shaded.

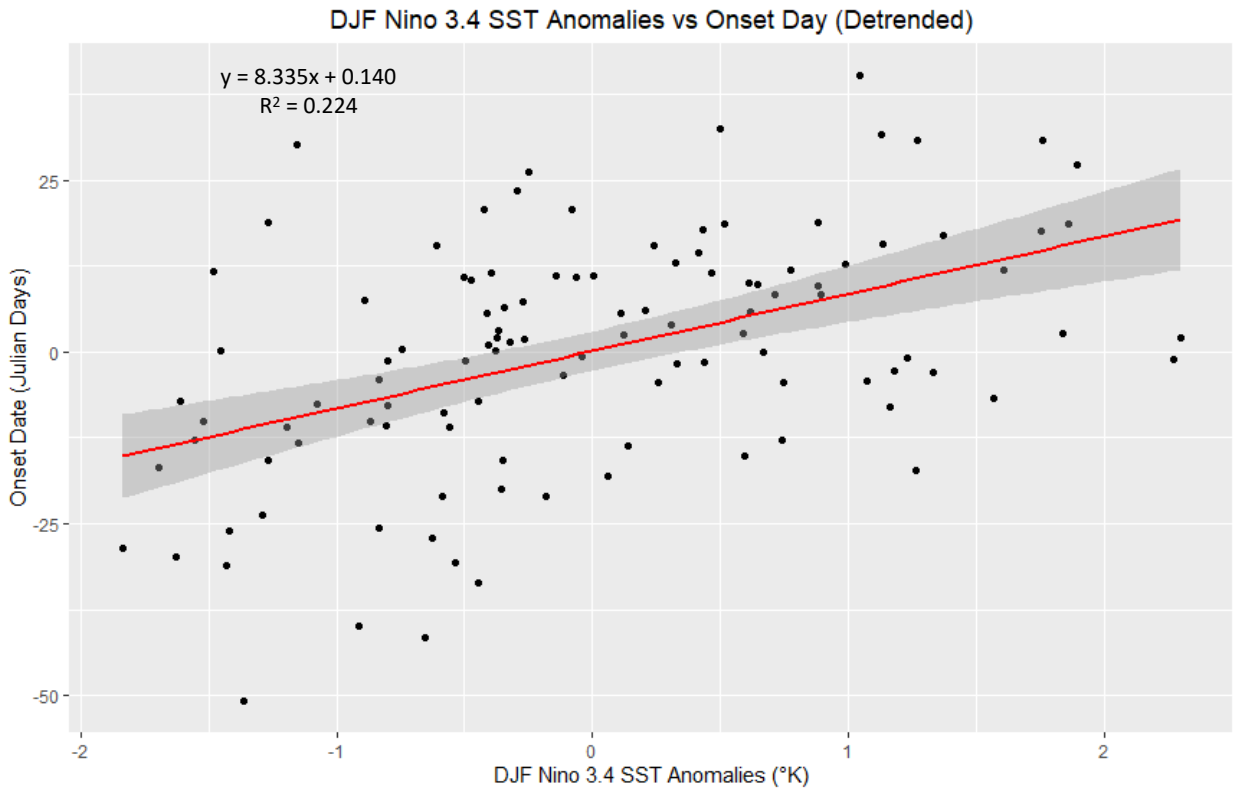

Figure 21: Scatterplot of the December through February Niño 3.4 sea surface temperature anomalies (in degrees °K) vs the onset day of the monsoon (in Julian Days). The R-squared value is shown on the figure as well as the least squares fit line of the data. Both time series have had their trends removed prior to plotting against each other. The 95% confidence interval for the regression line is shaded.

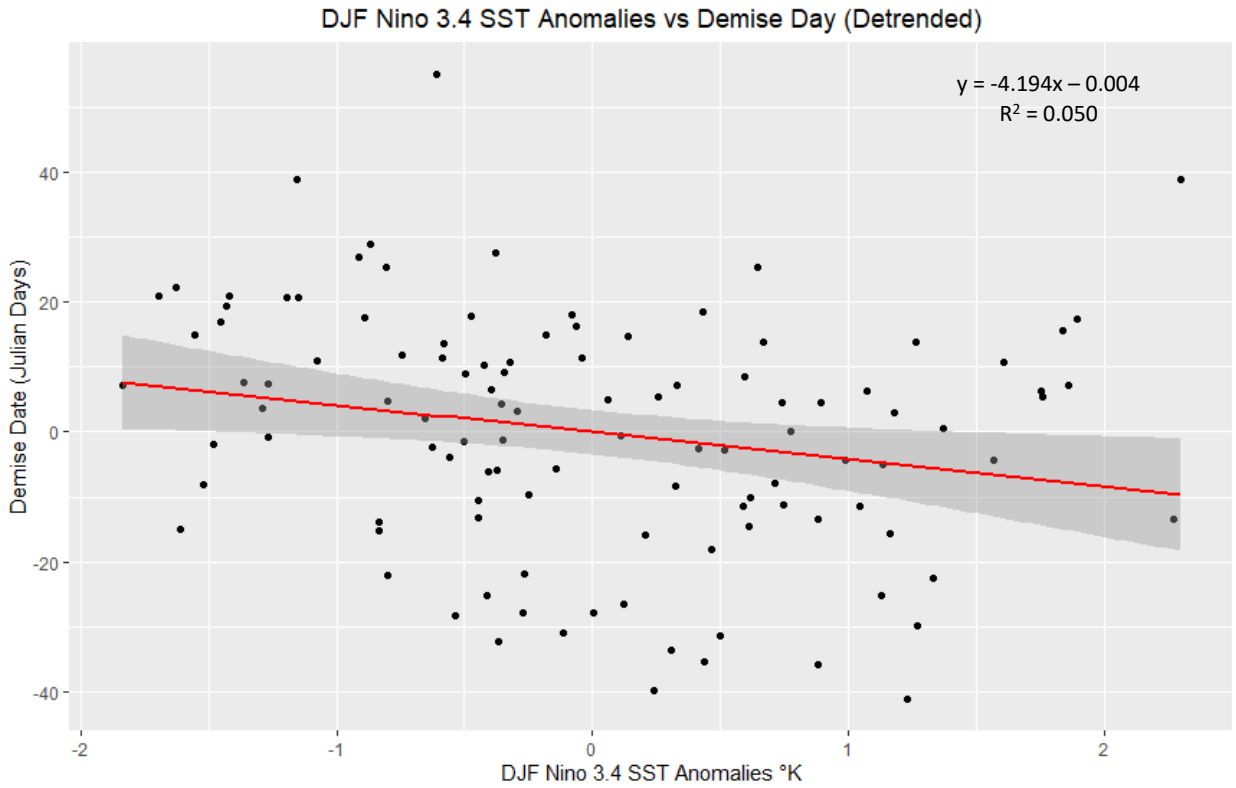

Figure 22: Scatterplot of the December through February Niño 3.4 sea surface temperature anomalies (in degrees K) vs the demise day of the monsoon (in Julian Days). The R-squared value is shown on the figure as well as the least squares fit line of the data. Both time series have had their trends removed prior to plotting against each other. The 95% confidence interval for the regression line is shaded.

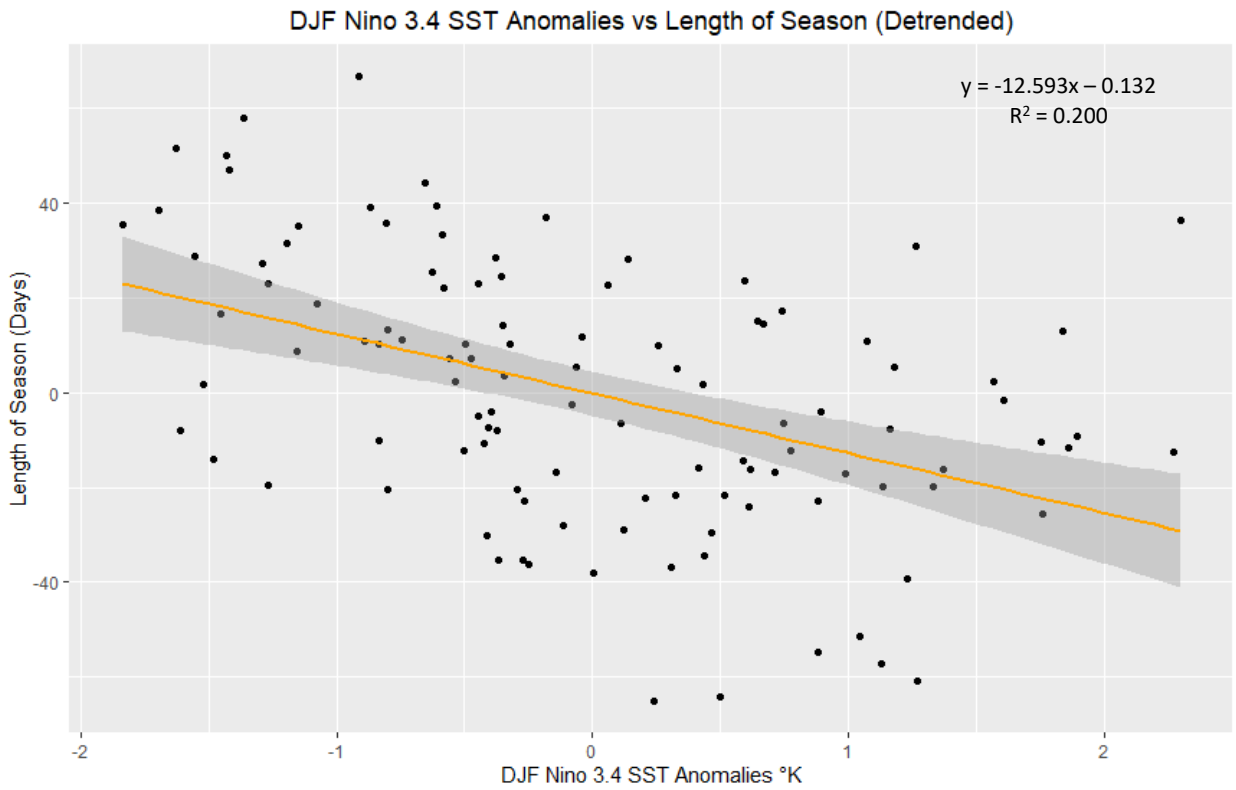

Figure 23: Scatterplot of the December through February Niño 3.4 sea surface temperature anomalies (in degrees K) vs length of the monsoon season (in days). The R-squared value is shown on the figure as well as the least squares fit line of the data. Both time series have had their trends removed prior to plotting against each other. The 95% confidence interval for the regression line is shaded.

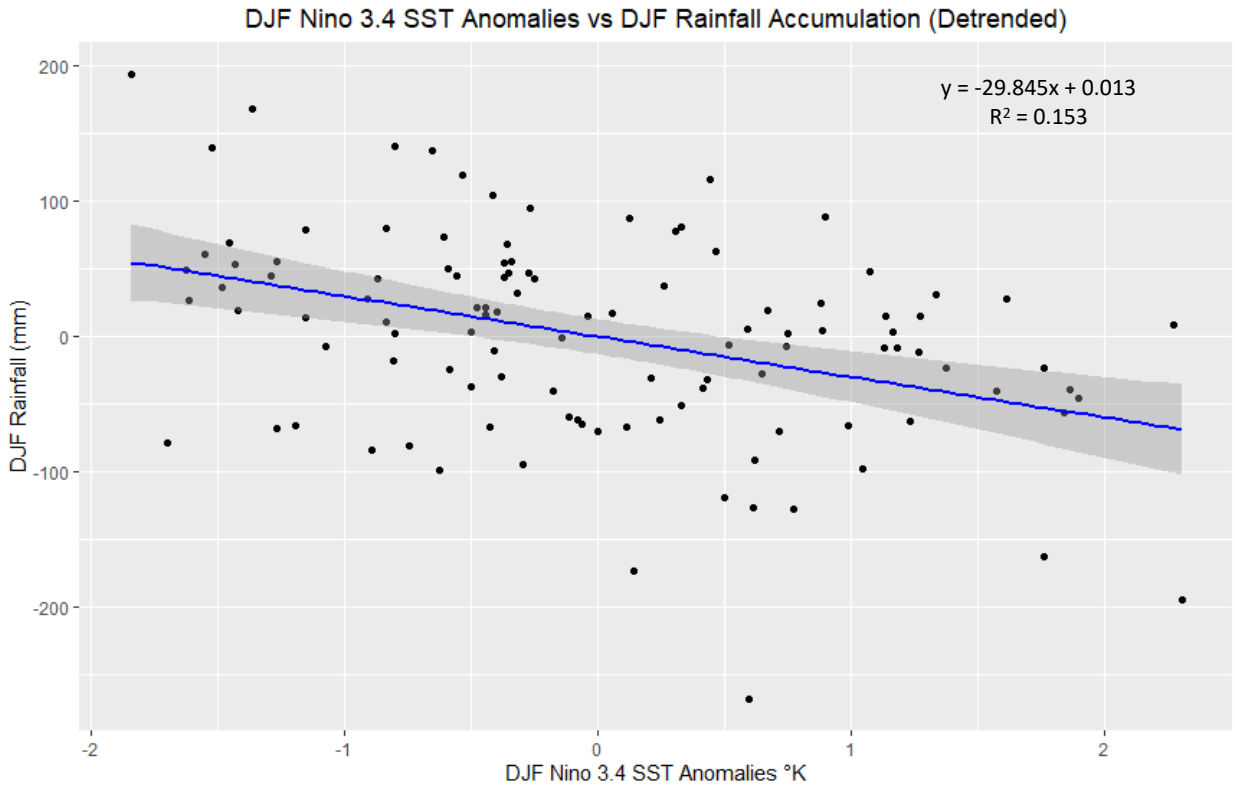

Figure 24: Scatterplot of the December through February Niño 3.4 sea surface temperature anomalies (in degrees K) vs area averaged total rainfall accumulation for December through February (in mm). The R-squared value is shown on the figure as well as the least squares fit line of the data. Both time series have had their trends removed prior to plotting against each other. The 95% confidence interval for the regression line is shaded.

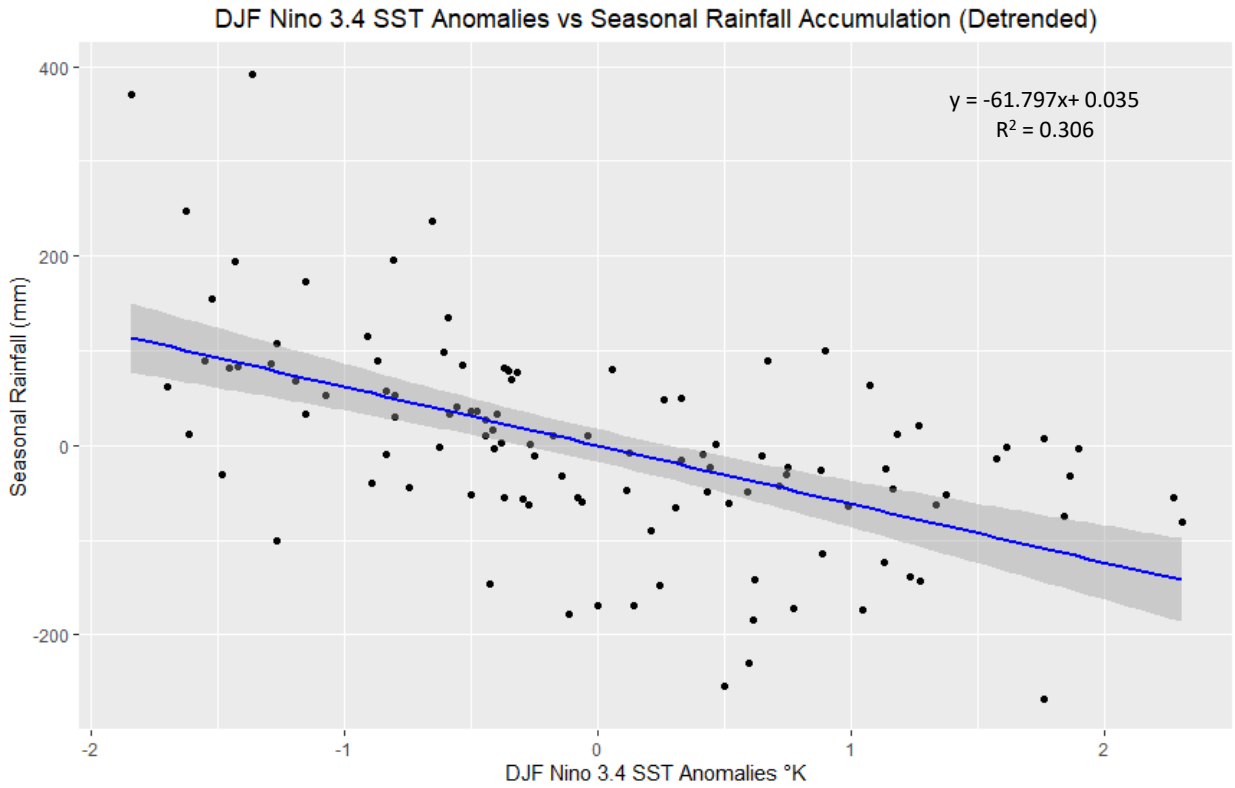

Figure 25: Scatterplot of the December through February Niño 3.4 sea surface temperature anomalies (in degrees K) vs area averaged total rainfall accumulation for each monsoon season (in mm). The R-squared value is shown on the figure as well as the least squares fit line of the data. Both time series have had their trends removed prior to plotting against each other. The 95% confidence interval for the regression line is shaded.

REFERENCES

Drosdowsky, W. 1996. Variability of the Australian summer monsoon at Darwin: 1957–1992. Journal of Climate 9: 85–96.

Flohn, H. 1960. Monsoons of the world. New Delhi (India Meteorological Department), 1960. Pp. x, 270, Figures; Tables. 12.00 Rupees. (1961). Quarterly Journal of the Royal Meteorological Society, 87(373), 460.

Grant, I. (2012, March 11). Daily Rain Gauge Precipitation (Rainfall) - Gridded, Australia coverage. http://data.auscover.org.au/xwiki/bin/view/Product+pages/Product+User+Page+Melbourne+2

Holland, GJ. 1986. Interannual variability of the Australian summer monsoon at Darwin: 1952-82. Monthly Weather Review 144: 594–604.

Joseph, P. V., and P. V. Pillai, 1988: 40-day mode of equatorial trough for long-range forecasting of Indian summer monsoon onset. Current Sci., 57, 951-954.

Jones D.A., Wang W., Fawcett R. (2009) High-quality spatial climate data-sets for Australia. Australian Meteorological and Oceanographic Journal 58, 233-248.

Kajikawa, Y. , Wang, B. and Yang, J. (2010), A multi-time scale Australian monsoon index. Int. J. Climatol., 30: 1114-1120. doi:10.1002/joc.1955

Kim KY, Kullgren K, Lim GH, Boo KO, Kim BM. 2006. Physical mechanism of the Australian summer monsoon: 2. Variability of strength and onset and termination times. Journal of Geophysical Research 111: D20105. DOI:10.1029/2005JD006808.

Li, J., Young-Min, Y., & Bin, W. (2018). Evaluation of NESMv3 and CMIP5 Models' Performance on Simulation of Asian-Australian Monsoon. Atmosphere, Vol 9, Iss 9, P 327 (2018), (9), 327. doi:10.3390/atmos9090327

Meehl, G.A.; Arblaster, J.M. The Asian-Australian monsoon and EL Nino Southern Oscillation in the NCAR climate system. J. Clim. 1998, 11, 1356–1385.

National Center for Atmospheric Research Staff (Eds). Last modified 08 Nov 2017. "The Climate Data Guide: Climate Forecast System Reanalysis (CFSR)." Retrieved from https://climatedataguide.ucar.edu/climate-data/climate-forecast-system-reanalysis-cfsr.

Nicholls N, McBride JL, Ormerod RJ. 1982. On predicting the onset of the Australian wet season at Darwin. Monthly Weather Review 110: 14–17.

Noska, R., and V. Misra (2016), Characterizing the onset and demise of the Indian summer monsoon, Geophys. Res. Lett., 43, 4547–4554, doi:10.1002/ 2016GL068409.

Renzullo, L., Chappell, A., Raupach, T., Dyce, P., Li, M., Shao, Q., 2011. An assessment of blended satellite-gauge precipitation products for Australia. CSIRO: Water for a Healthy Country National Research Flagship

Troup AJ. 1961. Variations in upper tropospheric flow associated with the onset of the Australian monsoon. Indian Journal of Meteorology and Geophysics 12: 217–230.

Villarini, G., P. V. Mandapaka, W. F. Krajewski, and R. J. Moore (2008), Rainfall and sampling uncertainties: A rain gauge perspective, J. Geophys. Res., 113, D11102, doi:10.1029/2007JD009214.

Wang B, Lin Ho, Zhang Y, Lu MM. 2004b. Definition of South China sea monsoon onset and commencement of the East Asia summer monsoon. Journal of Climate 17: 699–710.

Wyrtki, K. (1962). The Upwelling in the Region between Java and Australia during the South-East Monsoon. Marine and Freshwater Research, 13(3), 217.

Zhou T., Wu B., & Wang B. (2009). How Well Do Atmospheric General Circulation Models Capture the Leading Modes of the Interannual Variability of the Asian–Australian Monsoon? Journal of Climate, 22(5), 1159.

BIOGRAPHICAL SKETCH

Education:

Florida State University, Tallahassee, FL – July 2019

- M.S. Meteorology – GPA 3.7
- Thesis: Describing the onset and demise of the Australian Monsoon

University of Oklahoma, Norman, OK – December 2016

- B.S. Meteorology – GPA 3.6
- Dean's List (2014, 2016)

Professional Experience:

2018

- Arctic sediment core project
  Worked to assist a team from Oregon State University studying arctic sediment cores

2017-2019

- Teaching Assistant at Florida State University
  Helped with grading and course work for numerous meteorology classes

2015-2016

- Tutor
  Tutored peers at the University of Oklahoma for meteorology and math classes

2010-2012

- Youth Leader, St. Bonaventure Church
  Served as a coordinator and events leader for youth at St. Bonaventure Church

2005-2012

- Community Volunteer, BSA/Scouts Canada
  Eagle Scout
  Volunteered in my community on numerous occasions from 2005-2012